Testing and Analysis of Hybrid Magnetic Bearings

by

Robert R. Ambrogi

SUBMITTED TO THE DEPARTMENT OF
MECHANICAL ENGINEERING
IN PARTIAL FULFILMENT OF THE REQUIREMENTS
FOR THE DEGREES OF

MASTER OF SCIENCE IN MECHANICAL ENGINEERING

and

BACHELOR OF SCIENCE

at the

MASSACHUSETTS INSTITUTE OF TECHNOLOGY

June 1, 1987

© Robert R. Ambrogi

The author hereby grants MIT and Hughes Aircraft Company permission
to reproduce and distribute this document in whole or in part.

Signature of Author_____
Department of Mechanical Engineering
May 8, 1987

Certified by_____
Prof. Igor Paul, Sc.D.
Associate Professor, Mechanical Engineering
Thesis Supervisor

Accepted by_____
Prof. Ain Ants Sonin, Ph.D.
Chairman, Department Graduate Commitee

MASSACHUSETTS INSTITUTE
OF TECHNOLOGY
JUL 02 1987
LIBRARIES
ARCHIVES

Testing and Analysis of Hybrid Magnetic Bearings

by

Robert R. Ambrogi

Submitted to the Department of Mechanical Engineering in partial fulfilment of the requirements for the degrees of Bachelor of Science and Master of Science in Mechanical Engineering.

ABSTRACT

Testing and analysis was performed on a hybrid permanent and electromagnetic bearing in order to determine its performance constants. A negative spring constant of 1,550 lbs/in and a force constant of 103 lbs/amp were measured. Two axis measurements were performed to investigate cross axis coupling. Within the operating range of .003", the cross coupling as well as non-linearities in the spring and current fuctions were negligible. Coil inductances were also measured.

To correlate the experimental data, finite element and circuit analysis were performed. These methods predicted force and negative spring constants substantially higher than the experimental values. This discrepency is attributed to questionable magnet strength parameters. These analyses are good predictors of flux differentials, and given accurate magnet data, it is believed an accurate model can be created.

The bearing tested appears to be quite satisfactory for the magnetic suspension for which it was designed as well as for an actuated flexure system, which it may eventually be used in.

Thesis supervisor: Prof. Igor Paul
Title: Associate Professor, Mechanical Engineering

Acknowledgements

So many people contributed to this thesis it is impossible to name them all, however, I would like to give special thanks to:

- Stu Gassel, for chapmpioning this thesis and giving me the guidance and freedom needed to get it done.

- The Opto-Mechanical Engineering Department and The Mechanical Engineering Lab for financial support.

- Bowie Houghton, Ron Roche, John Daiber, and the PFC program for the use of their bearing and general magnetic know how.

- Nate, Hans, and the rest of the PM section for their interest, hints, and entertainment (especially Doug!).

- Allison Sheridan, Billy Kennedy, and Ed the Wheelhead for their Mac intelligence and the use of their machines.

- My parents, for everything.

Table of Contents

Acknowledgements..... 2

Table of Contents..... 3

List of Figures..... 5

List of Tables..... 7

Chapter 1: Introduction..... 8

1.1 Background..... 8

1.2 Project Description..... 12

Chapter 2: Magnetic Theory..... 21

2.1 Magnetic Materials..... 21

2.2 Magnetic Circuits..... 24

Chapter 3: Two Axis Testing of Magnetic Bearing..... 32

3.1 Test Objectives..... 32

3.2 Test Setup Description..... 33

3.3 Experimental Error..... 35

3.4 Test Procedures and Results..... 36

3.4.1 Negative Spring Contsant Tests (Small Gap) 36

3.4.2 Force Constant Tests (Small Gap)..... 40

3.4.3 Dynamic Tests (Small Gap)..... 42

3.4.4 Negative Spring Contsant Tests (Large Gap) 43

3.4.5 Force Constant Tests (Large Gap)..... 45

3.4.6 Dynamic Tests (Large Gap)..... 45

3.4.7 Gap Flux Measurements..... 48

3.5 Effect of Gap Size On Performance Constants..... 49

Chapter 4: Single Axis Tests..... 64

4.1 Test Setup..... 64

4.2 Static Testing..... 65

4.3 Dynamic Testing..... 67

Chapter 5: Finite Element Analysis..... 73

Chapter 6: Circuit Analysis..... 85

Chapter 7: Conclusions and Reccomendations..... 91

References..... 92

Appendix A: Physical Dimensions of PFC Demo Bearing..... 93

List Of Figures

1.1 - Two axis voice coil actuator..... 15

1.2 - Permanent magnet radial bearing..... 15

1.3 - Schematic of two axis, 4 pole magnetic bearing..... 16

1.4 - Actuated post flexure system..... 17

1.5 - Linear acting magnetic suspension..... 18

1.6 - PFC demonstration cross section..... 19

1.7 - PFC demonstration magnetic bearing..... 20

2.1 - Typical ferromagnetic material B-H curve..... 30

2.2 - Comparison between B-H curves of magnetically hard and soft materials..... 30

2.3 - Ferromagnetic demagnetization curve and shearing line..... 31

3.1 - Two axis test apparatus..... 50

3.2 - Small and large gap configurations - pole extensions..... 51

3.3 - Ball bearing stiffening of two axis apparatus..... 52

3.4 - Scan pattern for negative spring constant testing..... 53

3.5 - Force vs. position - no current..... 54

3.6 - Force vs. position - .2 amps X current..... 55

3.7 - Force vs. position - .1 amps X and Y current..... 56

3.8 - Force vs. current..... 57

3.9 - Voltage to force transfer function..... 58

3.10 - Voltage to force transfer function (cont.)..... 59

3.11 - Force vs. position - no current, large gap..... 60

3.12 - Force vs. position - .4 amps Y current, large gap..... 61

3.13 - Force vs. position - .4 amps X and Y current, large gap..... 62
3.14 - Force vs. current - large gap..... 63
4.1 - Single axis test apparatus..... 69
4.2 - Frequency response of 80% windings - series configuration... 70
4.3 - Frequency response of 80% windings - parallel configuration 71
4.4 - Frequency response of 20% windings - series and parallel configurations..... 72
5.1 - Small gap finite element model..... 80
5.2 - Large gap finite element model..... 81
5.3 - Flux plot, no displacement, no current case..... 82
5.4 - Flux plot, Two coils driven, no permanent magnets..... 83
5.5 - Flux plot, One coil driven, no permanent magnets..... 84

List of Tables

2.1 - Relative permeability of some common materials..... 22

3.1 - Negative spring constants for different off- axis positions, no current case..... 38

3.2 - Negative spring constants - .2 amp, X coils..... 40

3.3 - Negative spring constants - .1 amp, X and Y coils..... 40

3.4 - Force constants for various shaft positions and coil currents..... 41

3.5 - Small gap inductances, from voltage/current transfer function..... 43

3.6 - Negative spring constants - Large gap, no current..... 44

3.7 - Negative spring constants - .4 amps, X coil only..... 44

3.8 - Negative spring constants - .4 amps, both X and Y coils..... 45

4.1 - Small gap inductances, from voltage/ current transfer function and inductance bridge..... 68

5.1 - Finite Element Model Material Inputs..... 74

5.2 - Bearing Constants from Finite Element Analysis..... 76

5.3 - Comparison of Bearing Constants Between Finite Element Analysis and Experimental Values..... 79

6.1 - Gap flux density for various gap sizes..... 88

Chapter 1: Introduction

1.1 Background

As pointing system requirements get more stringent, the limits of the system begin to be determined by the limits of the mechanical bearings that support it. Mechanical bearings exhibit many non-desirable characteristics, including wear, a need for lubrication, a relatively high operating torque and torque noise, and runout. In order to get around these problems, much attention has been given to electromagnetic devices for supporting and actuating pointing systems. Because of their non-contact nature, electromagnetic bearings have excellent potential to provide precise positioning while maintaining vibration isolation [1]. There is also no wear or need for lubrication, giving them the potential to have extremely long lifetimes. Magnetic bearings also have the capability of operating at very low or high temperatures, although the performance of magnetic devices can change significantly over a wide temperature range.

Although magnetic levitation has been a topic of interest for over 150 years, recent interest has been caused by two main factors: the approach of the limits of mechanical technology, and the improvement of magnetic technology. Magnetic technology has improved in several areas: the development of high energy product permanent magnetic materials, the development of high saturation flux magnetic materials, and the improvements in microelectronics

and servo-technology [2]. As the technology improves, magnetic devices are becoming feasible replacements for mechanical bearings in certain applications.

Most magnetic devices apply force via one of three main operating principles: Lorentz forces, magnetic repulsion forces, or magnetic attraction forces. The Lorentz force, or "voice coil" device, is the oddball of the three types. Instead of generating force by magnetic flux alone, it generates force by passing current through a wire in a magnetic field. This type of device has much potential dynamically (which is why most loudspeakers use this principle, hence the name "voice coil"), but it tends to be limited in large force applications. A two axis voice coil actuator is shown in figure 1.1. Here two seperate windings pass orthogonally through a field set up by permanent magnets, thus generating "iL x ß" (Lorentz) forces in two directions.

The repulsion device, on the other hand, works on the priniciple that like magnetic poles repel. Magnetic poles are essentially flux sources or sinks, and they repel very similarly to groups of positive or negative electric charge. Since repulsion force increases as the poles approach, the pair has a positive stiffness. Thus it is stable in one degree of freedom, which is along the line connecting the two poles. Intuitively it seems that several repulsive pairs could be assembled in different axes to make a device stable in all degrees of freedom. However, the destabilizing stiffnesses in the cross axes are greater than the in-axis

stabilizing stiffness. What can result instead is a device that is unstable in all degrees of freedom. A suspension stable in all degrees of freedom cannot be built using only permanent magents. Earnshaw theorized this in 1852 [3], and he has yet to be proven wrong. Systems have been built with some of the axes supported with permanent magnets. One such device, developed by Backers [4], is shown in figure 1.2. Rings of alternating polarization magnets form a rotational bearing that is stable radially but unstable axially. A linear actuator and a control system are needed to keep the like polarized rings opposite each other to maintain radial stability.

The most promising type of device is the attraction device. Of the three, it has the potential to develop the most force per unit pole area [1]. Magnetic attraction occurs between any two pieces of magnetic material that have common lines of flux. The attraction force between the two materials is proportional to the square of the flux density in the gap that separates them. A 4-pole magnetic bearing, a typical attraction device, is shown schematically in figure 1.3. It is a hybrid permanent magnet and electro-magnet device developed by Wilson and Studor [3] that supports a shaft by creating flux in four gaps around the shaft. By varying the amount of flux in each gap, a net force is created to drive the shaft in whatever direction is desired. The bearing also has four permanent magnets to provide an initial amount of flux in each gap. There are coils wound around each pole to modulate this initial flux in order

to provide control. The bearing is configured in this way for several reasons. Because the initial flux is created by magnets instead of coils, the bearing consumes less power. This arrangement also improves the the linearity of the force vs. current function. Further, it also puts a larger effective air gap in the magnetic circuit (permanent magnets behave like air in a magnetic circuit), which lowers the inductance of the coils, which in turn improves the frequency response. The increased effective air gap reduces the force constant, however. Since this bearing is an attraction device, it is unstable. As the shaft approaches a pole, the flux in the gap increases, which increases the force generated by the gap. If there is no external resistance to this increase in force, the shaft pulls even closer to the pole, until it "crashes" on the pole face. Since it is unstable, there is a need for active control systems in both axes. The control systems modulate the flux in the gaps to keep the shaft in the desired position. The need for active control is a disadvantage of this type of bearing. It is also interesting to note that the maximum load capacity and stiffness of a servo-controlled magnetic bearing are ultimately determined by the servo system, rather than the bearing design.

As mentioned above, the attraction device exhibits the most potential for suspension and actuation applications; this report only investigates this type of device. A multi-pole actuator can be used in several suspension and actuation schemes. One, an actuated post flexure system, is shown in figure 1.4. A sensor package is mounted

on a post flexure, which can rotate about the flexure point in two axes. A two axis actuator, similar to the bearing shown in figure 1.3, is used to point the package. Using this scheme for fine pointing, several gimbal rings, rotary actuators, and bearings or flexures can be eliminated. This system also simplifies packaging, as the sensor package no longer has to be gimballed through its center of gravity.

In another application, figure 1.5 shows a cooler piston suspension system using two of the bearings shown in figure 1.3. The piston is suspended via two soft iron cores, which are in turn actuated by the two bearings. This particular system is designed for linear motion. The same arrangement can be used to support a rotating shaft, as would be the case in a gyroscope or a gimbal supension.

1.2 Project Description

The underlying purpose of this project is to investigate the performance of electromagnetic actuators/bearings for application in aerospace pointing systems. After some initial study, a studor bearing, similar to the device shown in figure 1.3, was chosen as the particular device to be analyzed and tested. There are several reasons for this. The Studor bearing is a relatively simple and versatile device. This particlular device also happened to be available at the time, thanks to the cooperation of the PFC program. Although one particular device is to be tested and analyzed, it is

hoped that this knowledge can be applied to magnetic devices in general, and thus expand our "electomagnetic intelligence" in regard to aerospace systems.

The Prototype Flight Cooler (PFC) program is a program to develop a long life cryocooler for space applications. In order to assure long life, it is designed with completely non-contacting compressor and displacer pistons. They are suspended magnetically and sealed with clearance seals. As a first step in building this cooler, a demonstration of the piston suspension was built. A sectional view of the demonstration suspension is shown in figure 1.6. It uses the Studor bearings shown in figure 1.3. The actual bearing, photographed in figure 1.7, is 11 inches in diameter by approx. 3 inches in thickness. The coils protrude roughly another inch on each side. It weighs approximately 50 lbs. The exact dimensions of this bearing are in Appendix A. This particular bearing is larger than neccessary in order to insure a successful suspension demonstration. The actual flight cooler bearing will be about half of the thickness and weight of this demonstration bearing. The large size and weight relative to mechanical bearings of equivalent load capacity are also disadvantages of electromagnetic bearings.

In the PFC cryo-cooler, the magnetic bearings must provide a sufficient force to levitate the compressor or expander piston in a gravitational field during ground testing and during small base accelerations in orbit. The bearings must also be controlled through

an acceptable bandwidth to respond to base motions and vibration. In order to determine the bearings suitability to this application, their performance characteristics need to be determined. Specifically, what is needed are the relationships between the bearing inputs, displacement and current, and its output, force. These relationships have to be determined both statically and dynamically. Although magnetic devices are inherently non-linear, this particular bearing has fairly linear behavior (ie., force vs. current) due to its design and relatively small operating range. Statically, two constants, the force constant and the negative spring constant, adequately describe the bearing performance. Dynamically, what needs to be determined is the frequency response, or more specifically, the coil voltage-to-force transfer function. Because the coils are essentially first order devices (simple L-R circuits), this function can also be described by a constant, the inductive (L/R) time constant. This time constant is related to the operating bandwidth of the device. As is implied in its name, the L/R time constant is determined by the inductance of the device divided by the resistance of its coils. Thus by measuring this constant and the coil resistance, the inductance can be determined. The measured inductance can then be correlated to theoretical values.

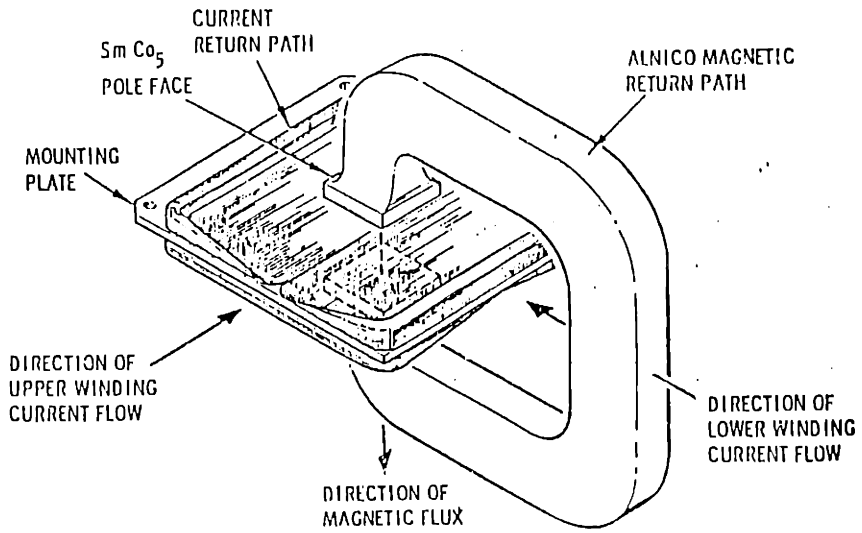

Figure 1.1 - Two axis voice coil actuator

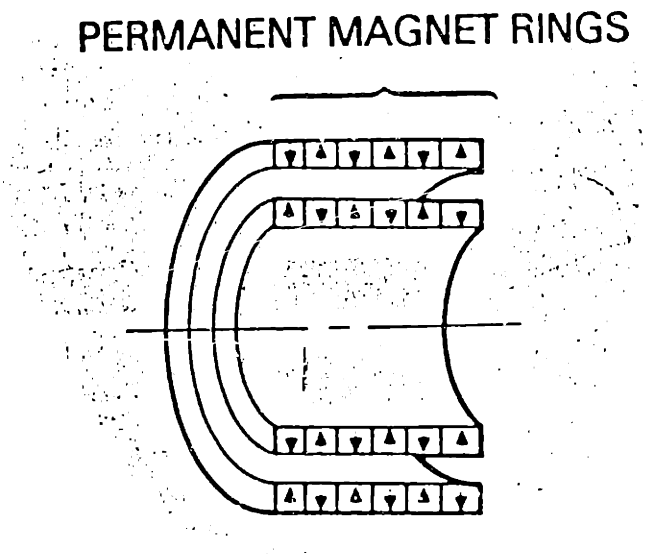

Figure 1.2 - Permanent magnet radial bearing

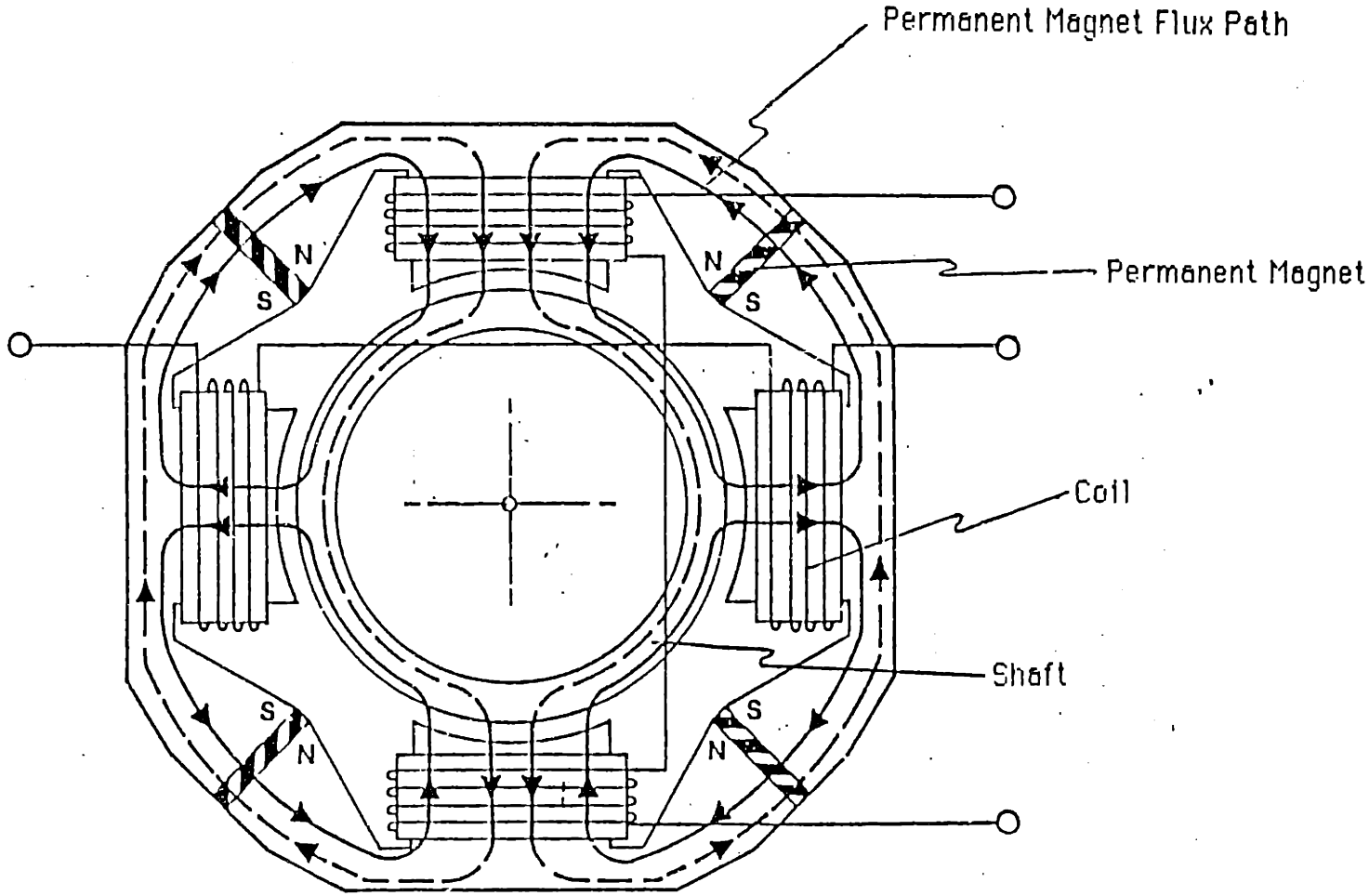

Figure 1.3 - Schematic of two axis, 4 pole magnetic bearing

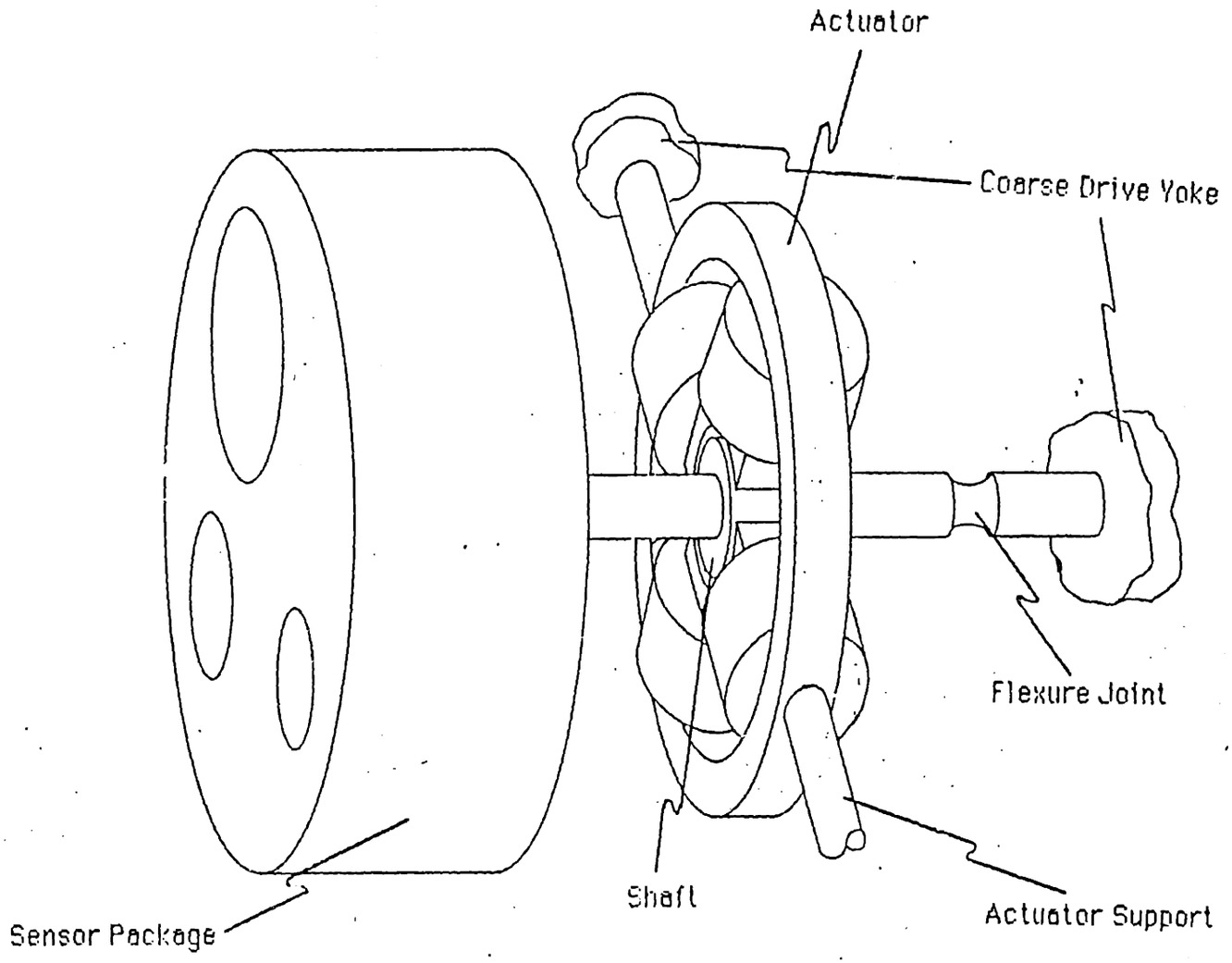

Figure 1.4 - Actuated post flexure system

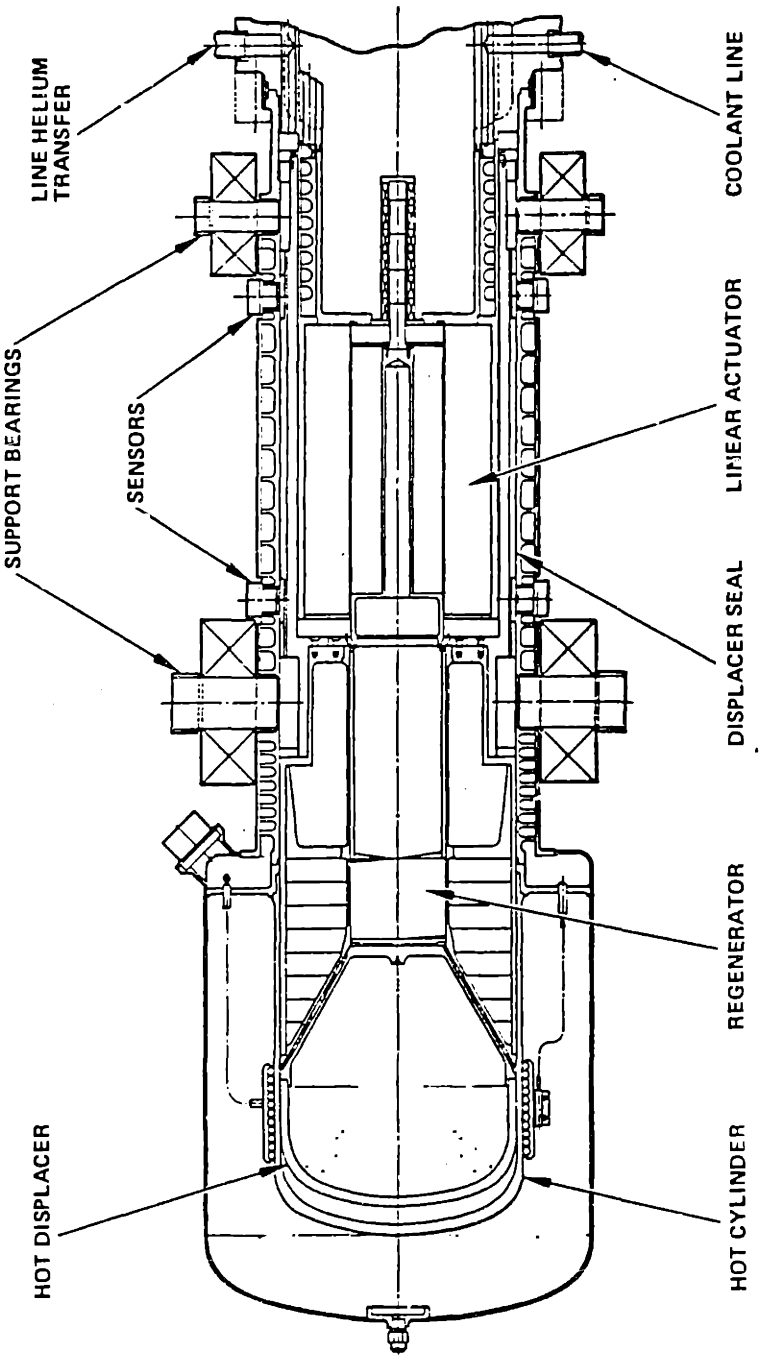

Figure 1.5 - Linear acting magnetic suspension

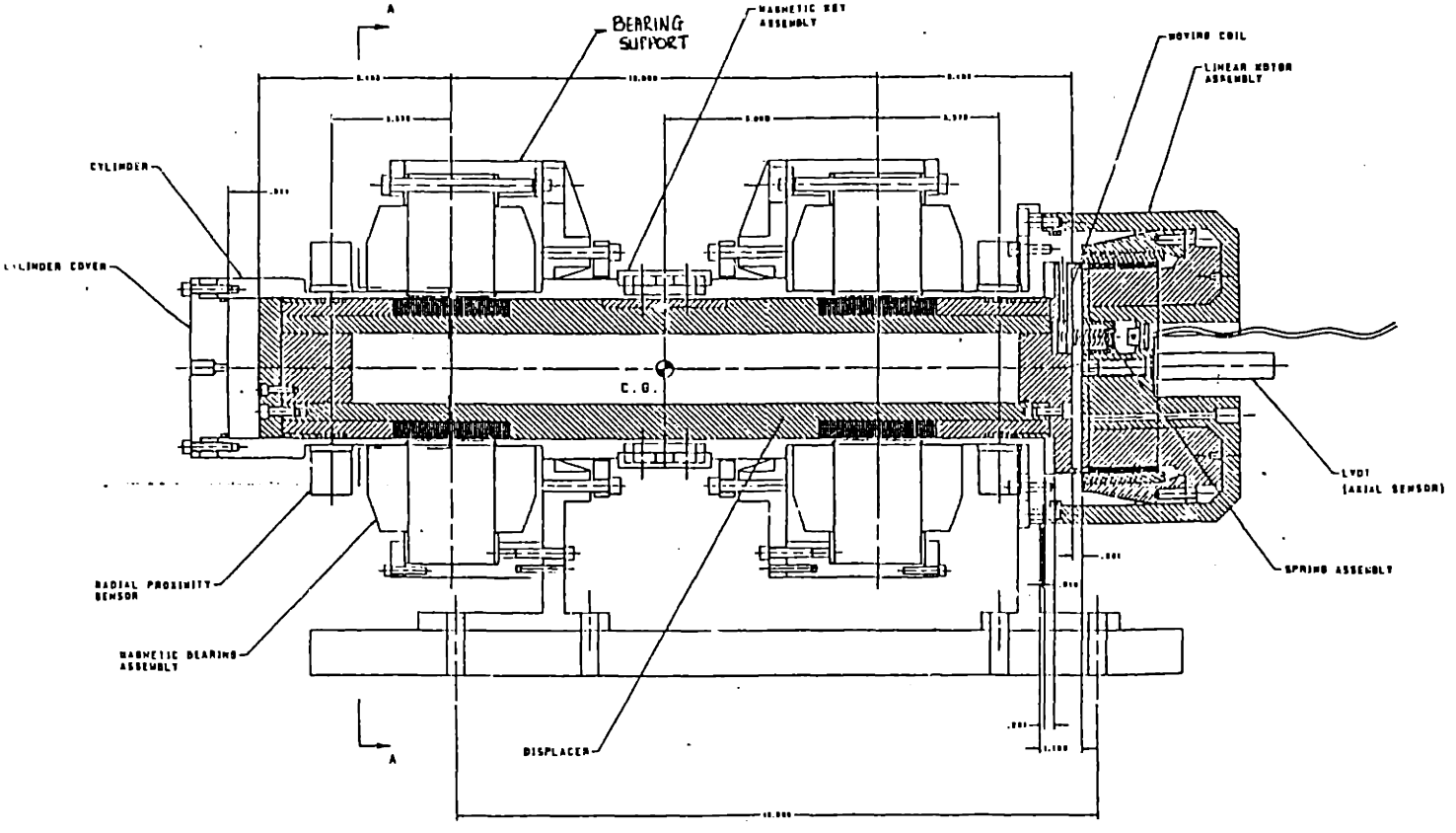

Figure 1.6 - PFC demonstration cross section

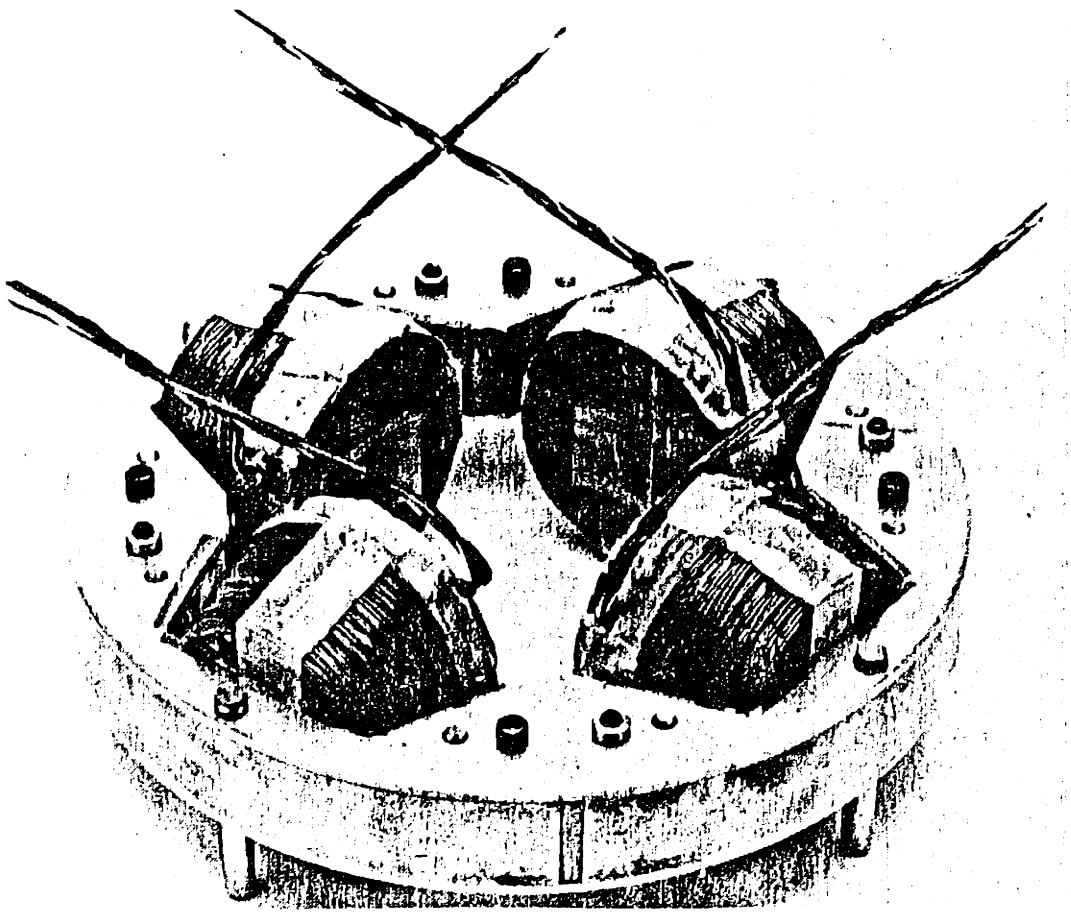

Figure 1.7 - PFC demonstration magnetic bearing

Chapter 2: Magnetic Theory

2.1 Magnetic Materials

All materials exhibit some magnetic behavior, of which there are several classes. Most common materials are either diamagnetic, paramagnetic, or ferromagnetic. In a diamagnetic material an external field induces a relatively weak opposing field, thus making the net field in the material less than the external field. If a diamagnetic material is placed next to a pole of a bar magnet, it will be reppelled from it. In a paramagnetic material the external field creates a weak field in the same direction as the external field. Thus the net field is slightly stronger than the external field. If a paramagnetic material is placed next to a bar magnet pole, it will be attracted to it. Although the only truly non-magnetic medium is a vacuum, some materials have have such minimal magnetic properties that they are considered non-magnetic. In fact, for the purposes of this project, all para and diamagnetic materials can be considered non-magentic.

Ferromagnetic materials, on the other hand, exhibit substantial magnetic effects. In these materials, the molecules easily align with the external magnetic field, creating a relatively strong field in the direction of the applied field. The net field strength in these materials can be thousands of times the strength of the applied field. These materials are very important in electromagnetic devices, as they are used to carry the working flux,

much as wires carry electric current.

An important characteristic of a magnetic material is its permeability, μ. This is the ratio of the applied field strength (H) to the net induced field strength (B). If the applied field strength is measured in amps per meter, and the induced field strength is measured in Webers per square meter, the units of permeability are Webers per amp - meter, more commonly known as Henries per meter. The permeability of a vacuum is 4π x 10E-7 Henries per meter; this value is the universal constant μ_o. The permeability of most materials is usualy measured relative to this value, refered to as the relative permeability, μ_r, which is dimensionless. The relative permeability of free space is 1 by definition. It is slightly less than 1 for diamagnetic materials, slightly greater than one for paramagnetic materials, and much greater than one for ferromagnetic materials. Table 2.1 lists the relative permeability of some common materials [7].

Table 2.1: Relative permeability of some common materials

Material	Type	μ_r
Bismuth	Diamagnetic	0.99983
Copper	Diamagnetic	0.999991
Vacuum	Non-magnetic	1.00
Air	Paramagnetic	1.0000004
Aluminum	Paramagnetic	1.00002
Mild Steel	Ferromagnetic	2,000.
Iron (0.2 impurity)	Ferromagnetic	5,000.
78 Permalloy (78.5 Ni)	Ferromagnetic	100,000.
Supermalloy (5 Mo, 79 Ni)	Ferromagnetic	1,000,000.

The relative permeability of para- and diamagnetic materials is fairly contant for different applied fields, while it is rarely constant for ferromagnetic fields. The permeability for these materials depends upon the specimen's history, as well as the applied field strength. The maximum permeability of the specimen is a material property, however. When the permeability of a ferromagnetic material is specified (as in the table above), this is what is usually being reffered to. Since μ_r varies, the magnetic behavior of the material is often instead described by it's B-H curve, which is a plot of the induced vs. applied field in the material. A typical B-H curve is shown in figure 2.1. The arrows on the curve show the history of the specimen's magnetization. The material starts at the origin, and B increases as H increases. Eventually B will not increase any further. At this point the material is said to be saturated. As the H field decreases, B field in the material will decrease, but it will retain some magnetism at H=0. This amount of magnetism is called the retentivity. It is also reffered to as the residual flux density or the residual inductance. By applying a negative H field the flux density in the material can be brought back to zero. The amount of H needed to do this is called the coercive force, or coercivity, of the material. These two numbers are important properties of permanent magnets. They describe the maximum flux density they can produce and how easily the material is demagnetized. As the magnetic field is again

applied, the B field in the material will increase, but along a different path than when the field was decreased. A hysteresis loop results. The area inside this hysteresis loop is the proportional to the work done on the material after it has been negatively and positively saturated. Materials which have a small hysteresis loop area (see figure 2.2) are said to be magnetically soft. They are useful as flux carriers, as little energy is lost during internal flux density cycles. Materials with large hysteresis areas are useful as permanent magnets, as they store more energy and are not easily demagnetized. The maximum product of B and H along the demagnetizing portion of the B-H curve is called the energy product of the magnet (see fig. 2.3). It is an indication of the energy stored, and hence the stength of the magnet. The magnets used in the bearing tested for this thesis were made of Samarium-Cobalt, a magnetically very hard material, with a retentivity of 0.965 tesla, coercivity of 716,000 A/m, and an energy product of 160,000O Oersted - Teslas [8].

2.2 Magnetic Circuits

An electric circuit forms a closed path through which current flows. Similarly, magnetic flux lines are continuous and form closed paths. Thus each flux line makes up a single magnetic circuit, and all flux lines from a given source taken in parallel also form a magnetic circuit. The amount of flux in a circuit is determined by the circuit's reluctance and the magnetomotive force

in the circuit. The magnetomotive force comes from sources such as coils (electromagnets) or permanent magnets.

The reluctance is determined by the permeability and geometry of the circuit. For a block of length l, cross sectional area A, and permeability μ, the reluctance to flux flowing along its length is given by the formula:

$$R = \frac{l}{\mu A} \qquad (2.1)$$

A magnetic circuit can be analyzed by summing the network of reluctances along the flux path, giving the total reluctance of the circuit.

Given a circuit with a known reluctance, we want to determine the flux density within the circuit created by a permanent or electromagnet. If the circuit consisted of a solid toroid with a coil wound around it, the flux density inside the coil could be calculated with the formula:

$$B = \frac{\mu N I}{l} \qquad (2.2)$$

where N is the number of windings around the toroid, I is the current in the winding, l is the circumference of the center of the

toroid, and μ is the permeability of the toroid material. The ratio μ/l is equal to $1/RA$, however. Substituting this into 2.2 gives:

$$B = \frac{N I}{A R} \qquad (2.3)$$

where A is the circuit cross sectional area and R is the total circuit reluctance. If I is in amps, A in square meters, and R in reciprocal Henries, B will be in Teslas. This equation can be used to calculate the flux density inside a circuit of constant cross sectional area. Since flux lines are continuos and closed, the total flux in any cross section must be a constant.v Thus the product B x A will be constant in a circuit with varying cross section.

Equation 2.3 allows us to calculate the flux density in an electromagnetic circuit, but a permanent magnet circuit must be handled much differently. This is because an electromagnet operates in the first quadrant of the B-H curve, while a permanent magnet works in the second quadrant. The permanent magnet's B-H curve in the second quadrant is known as the demagnetizing curve, shown in figure 2.3. First consider a todroid made up of a permanent magnet. Since there is no external field on the toroid, it would have an internal flux density equal to the material's retentivity. Few magnetic circuits are made up of only permanent magnets, however. When another material (air or soft iron for example) is inserted in the circuit the flux density drops to an operating point on the material's demagnetizing curve. The configuration of the magnetic

circuit will determine this operating point. For a circuit containing a permanent magnet and other materials such as soft iron poles and air gaps, there is a characteristic ratio between B and H within the circuit. This ratio can be plotted as a line on the B-H curve, known as the shearing line. The equation for the shearing line is given by:

$$\frac{B}{H} = -\mu_e \frac{l_m}{l_T - l_m} \qquad (2.4)$$

where l_m and l_T are the magnet and total circuit lengths, respectively. μ_e is the effective permeability of the circuit. For a circuit made up of iron poles and air gaps this is:

$$\mu_e = \frac{(l_{air} + l_{iron})\,\mu_{air}\,\mu_{iron}}{l_{air}\,\mu_{iron} + l_{iron}\,\mu_{air}} \qquad (2.5)$$

The permanet magnet's operating point, and hence the flux density within the circuit is the point where the shearing line and the B-H curve intersect. For a reasonably linear magnet this can be calculated, or it can be found graphically for non-linear materials.

The reason for calculating the flux density within a magnetic circuit is to find the force that the circuit can generate across a gap. All of the circuits in the bearing studied here have at least one air gap in them. When flux passes through one of these gaps it generates force between the two sides of the gap. The force (in

Newtons) between the poles is given by [7]:

$$F = \frac{B^2 A}{2 \mu_0} \qquad (2.6)$$

provided B , A, and μo are specified in MKS units. In the bearing tested, there are four opposing gaps that together can force the shaft in two directions. If all of the gap flux densities are equal, the net force on the shaft is zero. If the initial flux density in one gap is increased by an amount ΔB_c, and the opposite one decreased by the same amount, the net force on the shaft will be:

$$F = \frac{[(B_0 + \Delta B_c)^2 - (B_0 - \Delta B_c)^2] A}{2 \mu_0} \qquad (2.7)$$

Where B_o is the initial flux density. Expanding and cancelling, this reduces to:

$$F = \frac{2 A \Delta B_c B_0}{\mu_0} \qquad (2.8)$$

Equation 2.8 indicates that the force is proportional to both the change in flux and the initial flux. The initial flux density will be a constant dependent on the strength of the magnets and the bearing's geometry, however. So the relationship between ΔB_c and coil current and shaft displacement will determine the operating

characteristics of the bearing. If ΔB_c is a linear function of current and displacement, the bearing will operate linearly. Equation 2.3 indicates that ΔB_c is linear with current. It may also be coupled to displacement since reluctance is a function of displacement. The relationship between ΔB_c and dispalcement is not as clear. It is definitely nonlinear, but may be reasonably linear within the operating range of the bearing. By measuring force vs. displacement and current, ΔB_c wil be determined experimentally. This will be compared with theoretical values calculated using the equations developed here and also a finite element approach.

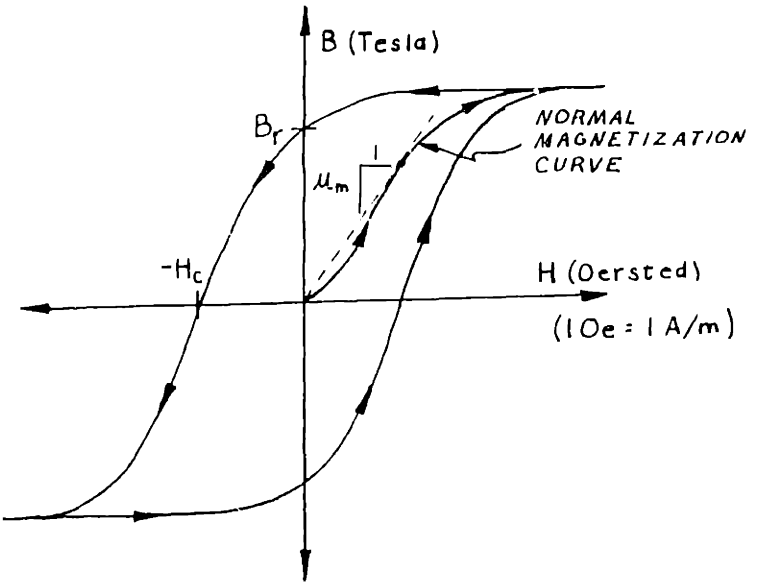

Figure 2.1 - Typical ferromagnetic material B-H curve

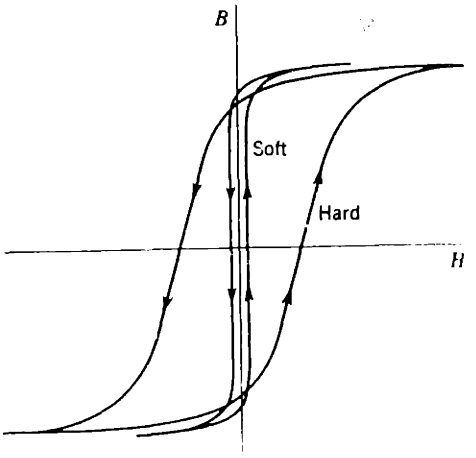

Figure 2.2 - Comparison between B-H curves of magnetically hard and soft materials

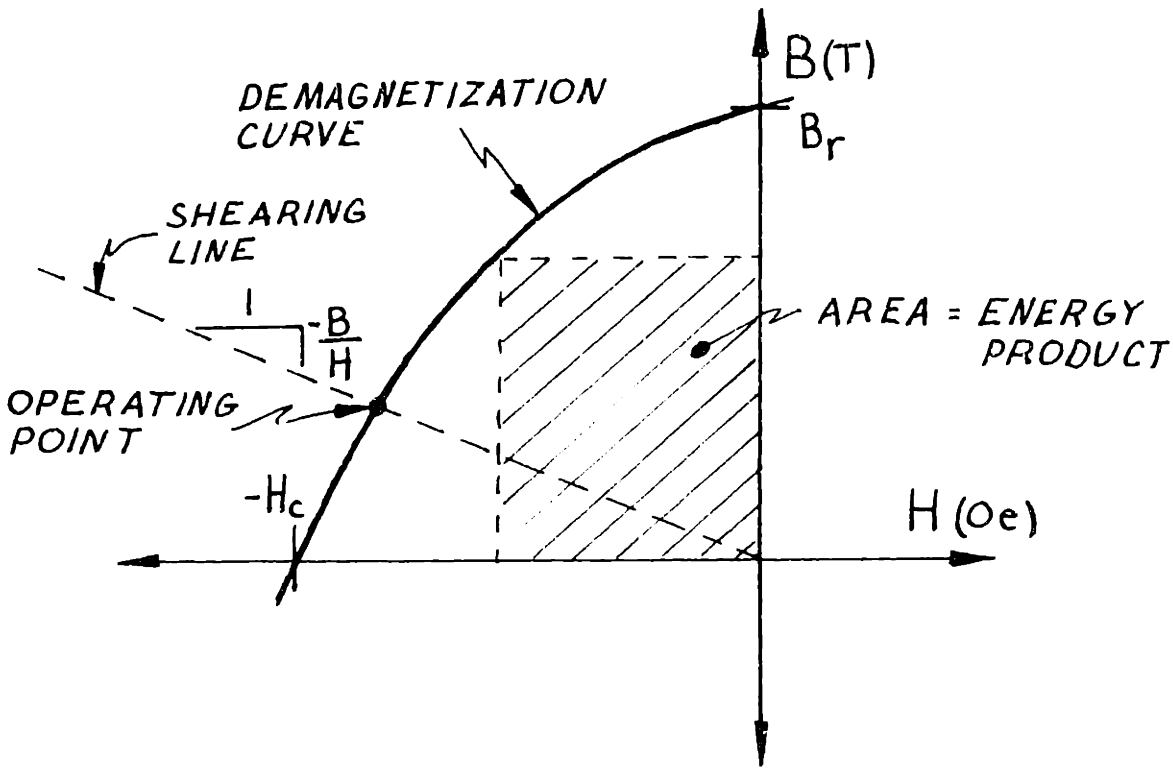

Figure 2.3 - Ferromagnetic demagnetization curve and shearing line

Chapter 3: Two Axis Testing of Magnetic Bearing

3.1 Test Objectives

The objective of these magnetic bearing tests is to determine the various operating constants of the bearing. Equally important as finding these constants however, is determining their dependence on the various inputs. More specifically, finding out the linearity and cross axis coupling of the bearing. Cross axis coupling is defined as the effects that one axis's inputs cause in the other. For example, when the shaft is moved in the Y direction, any change in the X axis negative spring constant would be considered "cross coupling". Knowledge of the cross coupling is important in designing the control systems for the bearing. The linearity of the device is also important for control purposes. In looking at the linearity, we want to determine how much the characteristic constants change over the operating range of the bearing. Specifically, what is to be determined are:

- the negative spring constant
- the force constant
- the L/R time constant and coil inductances
- the dependence of the above on shaft position and coil currents.

3.2 Test Setup Description

The test apparatus, shown in figure 3.1, consists of the bearing mounted on the multi-axis load cell via a fixture, which was then mounted on the jig borer table. The shaft was mounted in the jig borer spindle. By moving the borer table around, the shaft could accurately be located as desired in the bearing's magnetic field.

The test setup was designed to allow shaft movement and force measurement in both of the in-plane axes of the actuator. The main features of the test setup are the jig borer used to precisely locate the shaft between the poles, and the two axis load cell used to independently and simultaneously transduce the net force generated by each set of poles.

As the shaft is moved in-between the poles, the load cell measures the X and Y axis forces generated between the bearing and the shaft. A computer data aquisition system was used to record the forces during the tests. To keep load cell deflection from causing error in positioning, dial gauges were set up between the bearing and the shaft. Thus displacement of the shaft relative to the bearing was measured regardless of the load cell displacement. Another problem caused by load cell deflection was tilting of the entire bearing assembly. Since the force applied to the bearing was above the center of the load cell, a moment was applied to the load cell, which caused it to tilt (rotate). (The load cell used has a relatively low moment stiffness.) This caused unacceptable displacements, and also decreased the total load cell stiffness in

the in-plane directions to below the negative stiffness of the bearing. Thus the test apparatus was unstable, and the shaft could not be inserted without causing it to "crash" against the poles.

As a first order solution to this problem, the bearing's negative stiffness was reduced by removing the pole extensions and thus opening the air gaps. The poles on the bearings were designed to be ground flat, and then extensions would be put on to make the poles conform geometrically to the shaft (see fig. 3.2). With the extensions removed, the air gap increased from 0.065" to an effective air gap of 0.215". (The gap is non-uniform; 0.215" is the equivalent uniform gap.) Since negative stiffness varies as an inverse function of the gap length, the bearing is substantially less unstable without the pole extensions. Removing the pole extensions also allowed investigation of the effect of gap size on bearing performance, thus expanding the scope of this study.

In order to test the bearing with the pole extensions installed, it was necessary to increase the moment stiffness of the test rig. This was done by shimming up the extremities of the bearing fixture on blocks and ball bearings. (See figure 3.3) This allowed the bearing to translate in-plane, and thus allow the load cell to operate in-plane, but it did not allow the bearing to tilt. In this configuration, the load cell was stiff enough to restrain the bearing, and thus the test rig was stable. Constraining the load cell tilting also decreased X - Y cross coupling seen in the large gap tests.

3.3 Experimental Error

There were several sources of error in these tests. Most of them involved the load cell. Although it was designed to transduce forces and moments independently in all three axes, it did have some cross coupling. This cross coupling was not the same for all axes. It was linear and repeatable, however, so that it could be calibrated. As such, it was measured for both the X and Y axes, and subsequently removed from the data. The X axis had 4% of the Y axis value superimposed on itself, while the Y axis had 11% of the X value superimposed on it. These numbers are accurate to plus or minus 1%. The load cell also exhibited hysteresis. This was significant when large forces were applied to the load cell. To remove this error, most of the data was taken twice, loading in the opposite direction each time. These values were averaged together. Using this technique, the hysteresis was reduced to values well below the other errors. Without this technique, the hysteresis was as large as 2% of the indicated value. Since a digital voltmeter was used, and the data was recorded via computer, reading error was negligible. Positioning error was significant at times. Using the dial indicators to locate the shaft, absolute position was repeatable to plus or minus 0.001". This corresponds to a force error of 2.5 lbs. The absolute force error is only relevant at the maximum forces measured farthest from magnetic zero, as it is the maximum force that is used to calculate the negative spring constant. At the

maximum displacements, the 2.5 lb positioning force error is 5% of the measured force. Elswhere, it is the differential position accuracy which is important, since the slope of the force vs. displacement curve (Δforce over Δposition) is the true item of interest. Differential position was accurate to approximately 0.0002", which corresponds to a 0.5 lb error.

3.4 Test Procedures and Results

As mentioned above, the PFC magnetic bearing was tested in both a large gap and a small gap configuration. Because the small gap case is the actual operating setup, these results are dicussed first, in sections 3.4.1 - 3.4.3. The large gap results are presented in sections 3.4.4 - 3.4.6. The results are compared in section 3.4.7.

3.4.1 Negative Spring Constant Tests (Small gap)

To perform the negative spring constant test the shaft is moved around the bearing field, and the resultant forces are recorded at a variety of points. For the small gap tests the shaft was moved around a 9x9 grid of points, each point being 0.005 inches apart. A regular scan pattern was adopted in both cases. This is shown in figure 3.4. The field was scanned twice for each test, once in each direction. These two results were averaged together. This procedure removed the hysteresis in the load cell caused by its strain element and rubber seals. In some of the tests, it was not possible to run the scan pattern in both directions, and a

slight "rippling" of the data can be seen transverse to the scan direction.

Several different cases of negative spring constant tests were run. Current was varied for each of the cases to determine its effect on the negative spring constant. The first case run was with no current in the coils. Graphs of X and Y force versus position are shown in figures 3.5 and 3.6. These graphs show that the bearing is fairly linear (the force plane has roughly a constant slope in the direction of the force) and has little cross coupling (the force plane is flat in the transverse force axis). Table 3.1 lists the negative spring constants for each of the different off axis positions that were measured. From this we can see that the negative spring constant increases as the shaft travels off axis. At .020" the constant increases from ≈2,400lb/in on the magnetic zero axis to ≈2,630 lb/in. This is an increase of 9.5% over its on axis value. This is relatively minor, considering that the operating range is only a few thousandths from the magnetic center.

Table 3.1: Negative spring constants for different off-axis shaft positions - no current case.

Dist. from Ctr. (in)	-Kx (lb/in.)	-Ky (lb/in.)
-.020	2,470	2,690
-.015	2,390	2,580
-.010	2,360	2,510
-.005	2,340	2,480
.000	2,360	2,470
.005	2,380	2,480
.010	2,480	2,510
.015	2,540	2,580
.020	2,680	2,670

A plot of total radial force was also generated for each test (figure 3.7). Here the X and Y forces were added vectorially to obtain the total force outward radially from the magnetic center (the point of zero net force on the shaft). This plot shows that the greatest force outward is in a direction between the poles. Thus, when the bearing crashes it will tend to crash against two poles rather than one. It is also interesting to note that the radial force is constant for a given radial distance from the magnetic center. Even though the bearing operates in a cartesian fashion (actuating in X and Y axes), it has a decoupled radial behavoir (ie. radial force varies with R but not with Theta).

Two tests were run with current in the coils. One was with .2 amps of current in just one axis' coil, the other had .1 amps of

current in the coils of both axes. These results are shown in figures 3.8 through 3.11. The data appears somewhat rougher and rippled in these cases. This is because only one data set was able to be taken for each case due to problems with crashing*. In both cases, the negative spring constant does not change significantly with the application of current. The current merely shifts the magnetic center point of the bearing. This can be seen most clearly in the radial plots, where the low point of the surface is the magnetic center. A current in the X direction moves the center in the X direction, and likewise for Y. Again, an increase in the force (and hence the negative spring constant) is seen as the shaft moves in the transvers axis. It appears even more pronounced in these cases because the magnetic center is shifted. Although the shaft is in the same position as in the no current case, it is effectively closer to the pole due to the increased gap flux from the coil current. The cross coupling and non-linearity tend to increases as the gap flux does. The negative spring constant increases from ≈2,380 lbs/in. on the axis to ≈2,680 lbs/in. at .020" off the axis, a 13% increase.

* In the case of the negative spring constant tests with current in the coils, the coils were driving the shaft toward one of the poles. As the shaft approached this pole, the force was large enough that the test rig was near the edge of its stability region. It was relatively easy to bring the core from a low force region near magnetic center to the high force region near the pole, but extremely difficult to work back from near the pole towards magnetic center. On all occasions that this was tried the pole crashed against one of the poles. This problem can attributed to a combination of lack of stiffness in the test rig, hysteresis, and positioning error.

This is a greater increase than in the no current case. Table 3.2 lists the negative spring constants for the test run with .2 amps in the X coil, table 3.3 lists the same for the test with .1 amps in both the X and Y coils.

Table3.2: Negative spring constants - .2 amps, X coils

Dist. from Ctr.	-Kx (lb/in.)	-Ky (lb/in.)
.020"	2,580	3,120
.010	2,420	2,750
.000	2,380	2,640
-.010	2,504	2,620
-.020	2,780	2,670

Table 3.3: Negative spring constants - .1 amps, both X and Y coils.

Dist. from Ctr.	-Kx (lb/in.)	-Ky (lb/in.)
.020"	2,510	2,840
.010	2,360	2,783
.000	2,360	2,690
-.010	2,520	2,712
-.020	2,790	3,080

3.4.2 Force Constant Tests (Small gap)

In the force constant tests, not only is the force constant desired, but also its dependence on shaft position and cross axis current. For this test the core was kept in one position, the current

was varied in a series of steps, and the force was recorded at each one. This was repeated for 3 different on-axis core positions, one off-axis core position, and a cross- axis current of .5 amps. Figures 3.12 through 3.16 show the force vs. current plots for each of these tests. Table 3.4 lists the force constants for each test. The force constant appears to vary very little with movement within the driven axis. (The axis that had its coil actuated.) The force constant does vary slightly with movement in the cross axis and with cross axis current. With no cross axis displacement or current, the force constant is between 133 and 136 lbs/amp. With a .020 inch Y axis displacement, the X axis force constant is 146 lbs/amp, an increase of 7%. With a .5 amp Y axis current, the X axis force constant is 128 lbs/amp, a decreas of 6%. Within load cell error, the non driven axis showed no variance as current was varied in the driven axis, ie. there was no force cross coupling.

Table 3.4: Force constants for various shaft positions and coil currents.

X (in)	Y (in)	Ix (amps)	Iy (amps)	Kf (lb/amp)
.000	.000	-.7 — +.7	0.0	136
.010	.000	-.5 — +.5	0.0	133
.020	.000	-.3 — +1.0	0.0	136
.020	.020	-.3 — +1.0	0.0	146
.000	.000	-.5 — +1.0	0.5	128

3.4.3 Dynamic Tests (Small Gap)

In order to measure the bearing's inductive time constant and hence its impedance, a series of dynamic tests were run. In the initial tests, coil current amplitude and phase, and resultant force amplitude and phase were measured against the input voltage for a variety of frequencies. From this the respective transfer functions could be derived between any combination of force, current, or voltage. On closer inspection, however, it was found that current and force are always in phase and are proportional. This is to be expected; moving electrons (current) generate magnetic flux, and magnetic flux generates force. These phenomena occur instantaneously. Thus, after this initial test, only the current vs. voltage transfer function was monitored. This simplified the test procedure, as only a current probe was needed rather than a dynamic multi-axis force transducer. For the initial tests, the transfer function was derived by inputting discrete frequencies. Later a spectrum analyzer was used with a white noise generator. This was used merely to speed up the testing, as all frequencies are tested at once. The coils were current driven with periodic white noise (made up of equal amounts of all frequencies over the test band for any given sample time). The spectrum analyzer used this and the output voltage spectrum to generate a transfer function. A variety of coil combinations were tested. A phase and amplitude vs. frequency plot

for each one is shown in figures 3.17 through 3.23. On these graphs, the 45 deg. phase shift point as well as the -3dB point define what is called the break frequency. In a first order system, the break frequency is the inverse of the L/R time constant. Thus by measuring the coil resistance, the coil inductance can be derived. The calculated coil inductances are listed in table 3.5. On the average, the inductances measured here are higher (by roughly a factor of two) than ones previously measured or calculated.

Table 3.5: Small gap inductances, as determined from voltage/current transfer function.

Coils	Config.	Break Freq (Hz)	t (m sec)	R (Ω)	L (Hy)
80%	series	.80	199	6.24	1.24
80%	parallel	.80	199	1.56	0.310
20%	series	3.84	41.4	1.62	0.067
20%	parallel	4.60	34.6	0.41	0.014
80%	single	0.96	166	3.12	0.518
20%	single	4.80	33.2	0.82	0.027

3.4.4 Negative Spring Constant Tests (Large gap)

The negative spring constant tests for the large gap configuration were run the same way as the small gap tests. The shaft was moved around through the same scan pattern, however the distance between each point was 0.020" instead of 0.005", used in the small gap case. Due to the lower negative spring constant, larger travel was needed to get reliably measureable forces. Again two sets of data were taken and averaged for each test to cancel the

load cell hysteresis. Three current cases were run: no current in either axis, .4 amps in one axis, and .4 amps in both axes. Figures 3.24 through 3.29 show X and Y force vs. position for these tests. In all three cases the graphs show that the bearing is extremely linear and non cross-coupled in the large gap configuration. Tables 3.6 - 3.8 list the negative spring constants for the off axis positions measured. For example, in the no current case, the X axis negative spring constant increases from 151 lb/in on the axis to 158 lb/in at 0.080" off the axis, an increase of 4.6%. Radial force plots are shown in Figures 3.30 - 3.32. Here we can see that the .4 amp coil current shifts the magnetic center ≈0.060" in both cases.

Table3.6: Negative spring constants - Large gap, no current

Dist. from Ctr.	-Kx (lb/in.)	-Ky (lb/in.)
.080"	158	156
.040	152	151
.000	151	149
-.040	153	151
-.080	158	156

Table3.7: Negative spring constants - .4 amps, X coil only

Dist. from Ctr.	-Kx (lb/in.)	-Ky(lb/in.)
.080"	149	165
.040	144	160
.000	144	158
-.040	148	160
-.080	155	166

Table3.8: Negative spring constants - .4 amps, both X and Y coils

Dist. from Ctr.	-Kx (lb/in.)	-Ky (lb/in.)
.080"	162	173
.040	153	163
.000	149	157
-.040	149	156
-.080	152	159

3.4.5 Force Constant Tests (Large gap)

Again the large gap force constant tests were fundamentally the same as the small gap tests. The pole was placed in four positions, three on-axis and one off-axis, and current was varied at each position. No cross axis current cases were run. Graphs of force vs current for each case are shown in figures 3.33 - 3.36. The force constants ranged from 24.4 lbs/amp to 26.1 lbs/amp. Although the high value was the case where the core was displaced off axis, it is only slightly higher, and within the range of the experimental error of the other values.

3.4.6 Dynamic Tests (Large gap)

Two dynamic tests were done while the bearing was in the large gap configuration. First the coil transfer function was measured, and then coil inductances were measured via coil reactance. For the transfer function measurements, discrete frequencies were inputted via a function generator. The current to

voltage ratio and phase lag were measured with an oscilloscope. Phase and amplitude measurements on an oscilloscope are quite difficult to do accurately, thus a reading error of 10 - 20% is likely in these measurements. The data from these tests indicates a break frequency of roughly 1.5 hertz, which corresponds to a time constant of 106 miliseconds. The coil resistance was 6.24 Ω, which indicates and inductance of 0.662 henrys. Because of the tedious nature of the test and its inherent innacuracies, the only case tested was the large coil (80%) winding. As a result of the difficulty in obtaining this transfer function, the spectrum analyzer method was developed for use in the small gap configuration.

As another method for determining inductance, coil reactance measurements were made using an AC power supply, a resistor box (a variable resistance where the resistance can be specified digitally), and a voltmeter. The coil and resistor box in series were driven with the power supply at a fairly high frequency (either 200 or 2000 Hz, depending on the winding). With the resistor box set at 0 Ω, the voltage across the coil was measured. The resistance was increased until the voltage across the coil dropped by half. The resistance of the box thus equalled the impedance of the coil at that driving frequency. With this the inductance of the coil can be calculated. At 200 Hz the 80% windings in series showed a 1213 Ω reactance. This corresponds to an inductance of 965 mH (milihenrys). The 20% windings in series had a 611 Ω reactance at 2000 Hz. This indicates an inductance of 48.6 mH.

Although the voltage/current transfer function and the reactance both measure inductance, the two methods sometimes do not agree. Actually the methods work on precisely the same principle. As the frequency increases, a greater voltage is needed to drive a given current through the inductance. That is, its impedance increases with frequency. If this is a first order system, one can calculate the inductance with any one impedance (or reactance) at a specific frequency. This is what is done in the reactance method. Or one can calculate the inductance by looking at the impedance as it varies over all frequencies. This is what is done in the transfer function method. By measuring the reactance, only one point on the transfer function is being measured and assumptions are being made about the rest. No first order assumptions need to be made with the other method, where the system order can be determined by looking at the transfer function. Thus the transfer function method is the more reliable of the two tests. In most cases, the purpose in determining the inductance is to determine the break frequency. That can be measured directly by measuring the transfer function or indirectly by measuring reactance and calculating it. An emphasis is placed on inductance in this report because it is the best number to use to match theoretical calculations. Because the reactance was measured at higher than operating frequencies, second order effects (such as capacitance between the individual coil wires) could have introduced error in the inductance measurement. Thus reactance should be used only as "quick and dirty" method of getting

inductance. It should also be done within the device operating frequency range. To obtain a clear indication of impedance vs. frequency, a transfer function should be measured.

3.4.7 Gap Flux Measurements, Large and Small Gap Configurations

For each configuration, the gap flux was measured with a gaussmeter. In the small gap case the initial (no current, no displacement) gap flux density was approximately 5,400 kilogauss (kG) in all four gaps. Because of the variance of flux density over the gap and the uncertainty of the probe position, these flux numbers contain possibly as much as 10% error. With 2.0 amps in one set of coils, the two driven gaps were driven to roughly 0 kG and 10.2 kG. The non-driven gaps remained at 5.1 kG and 5.3 kG. The gap flux was not measured as a function of shaft displacement.

In the large case the gap flux was measured both as a function of current and displacement. Because the gap was larger and non-uniform, there was more fringing on the gap perimeter, and hence greater flux density variance over the gap. The numbers given here represent average values, however they may be as much as 10% to 15% erroneous. The initial gap flux density was 2.35 kG. A current of .5 amps drove one gap up to 3.00 kG while pulling the other down to 1.73 kG. Similarly, a 0.040" displacement increased one gap to 2.82 kG and decreased the other to 1.98 kG. These numbers will be correlated with computer generated values in

section 5.

3.5 Effect of Gap Size on Performance Constants

In changing the gap spacing from 0.215" to 0.065", the gap was decreased by a factor of 3.31. The increase in gap size causes a significant decrease in the force and negative spring constants. The force constant decreased from ≈ 135 lbs/amp to ≈ 25 lbs/amp, a decrease of a factor of 5.4. Similarly, the negative spring constant decreased from ≈ 2,500 lbs/in to ≈ 150 lbs/in, a decrease of a factor of 16.6. Due to the measurement uncertaintanty, no conclusive relation can be drawn between gap size and inductance other than the fact that inductance will decrease as the air gaps increase. Thus, and unfortunately so, no solid conclusions can be drawn between gap size and bearing performance. The theoretical relations will be discussed in sections 5 and 6.

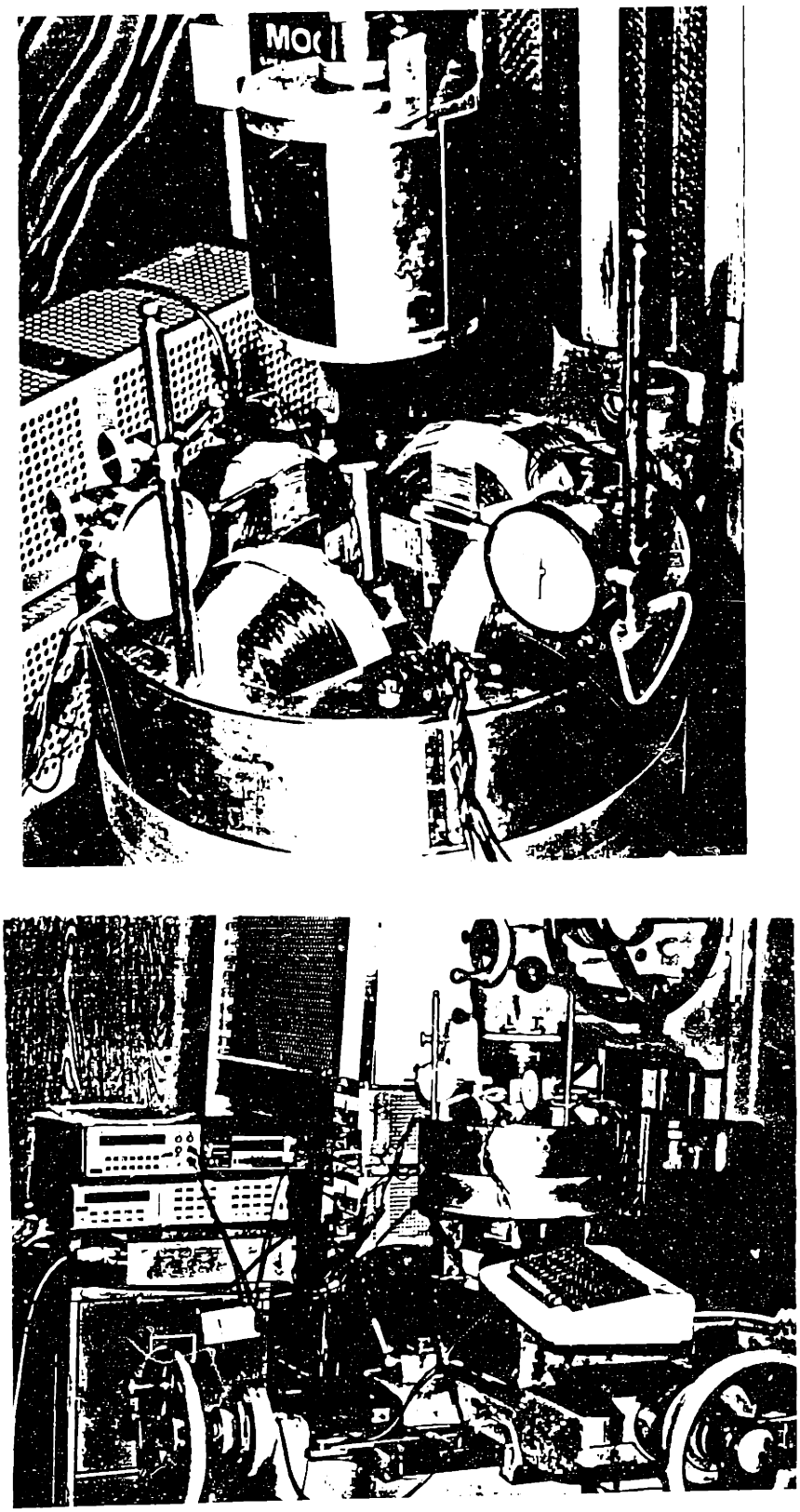

Figure 3.1 - Two axis test apparatus

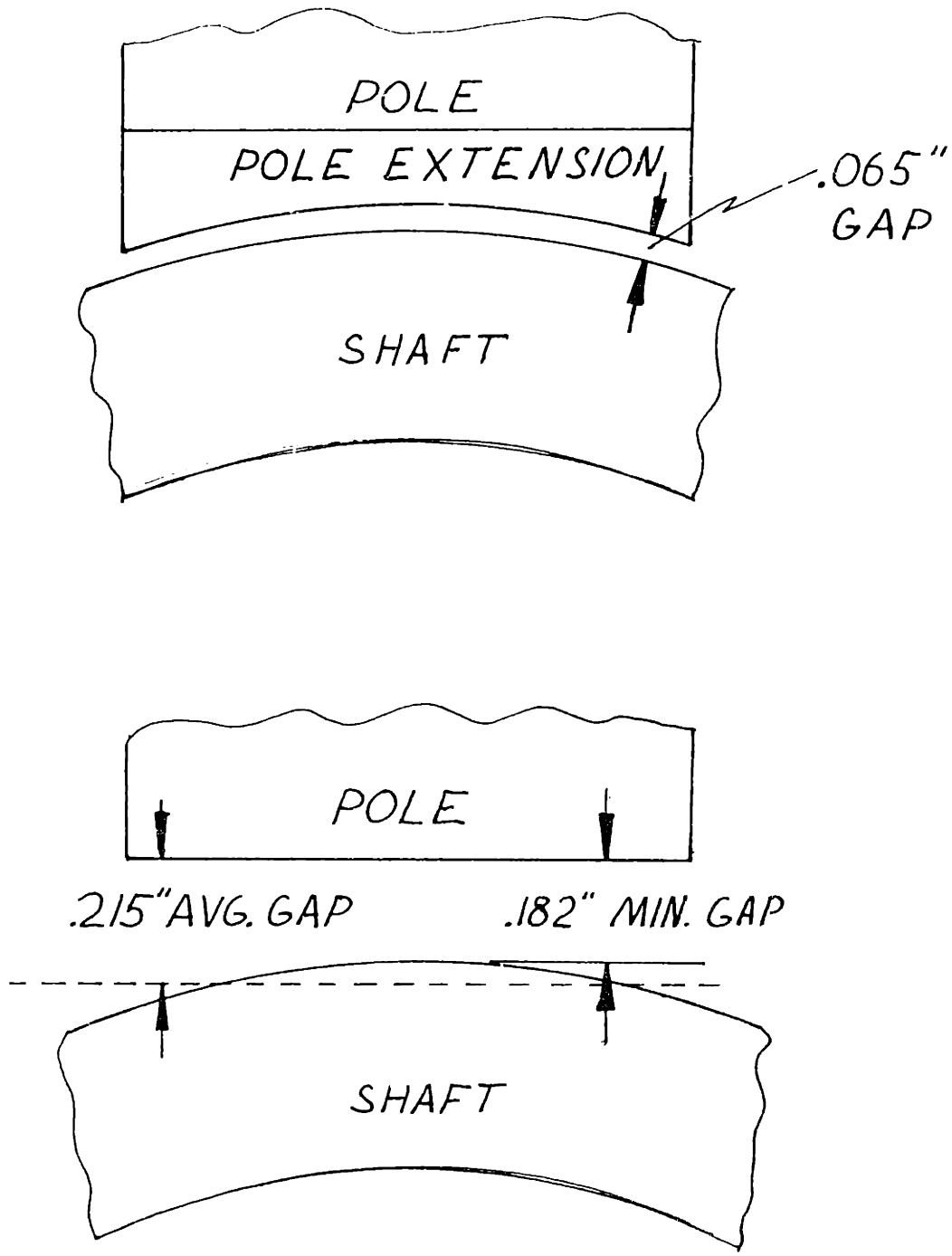

Figure 3.2 - Small and large gap configurations - pole extensions

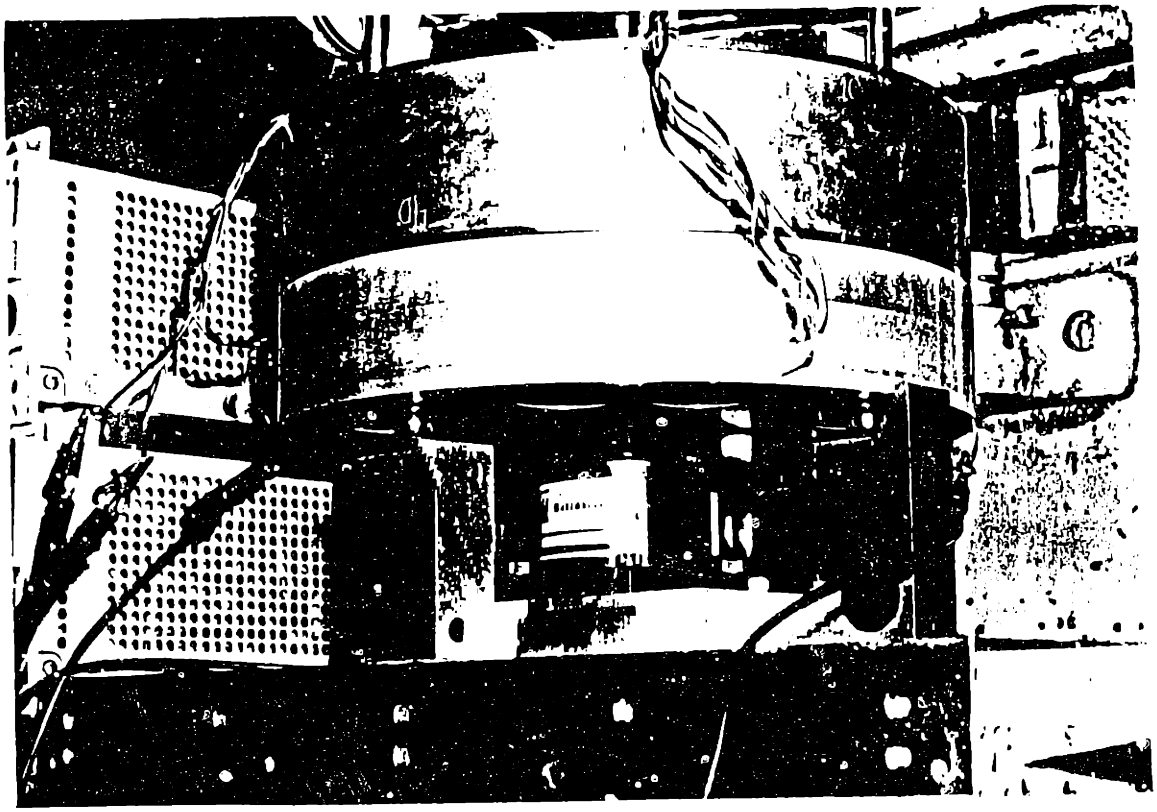

Figure 3.3 - Ball bearing stiffening of two axis apparatus

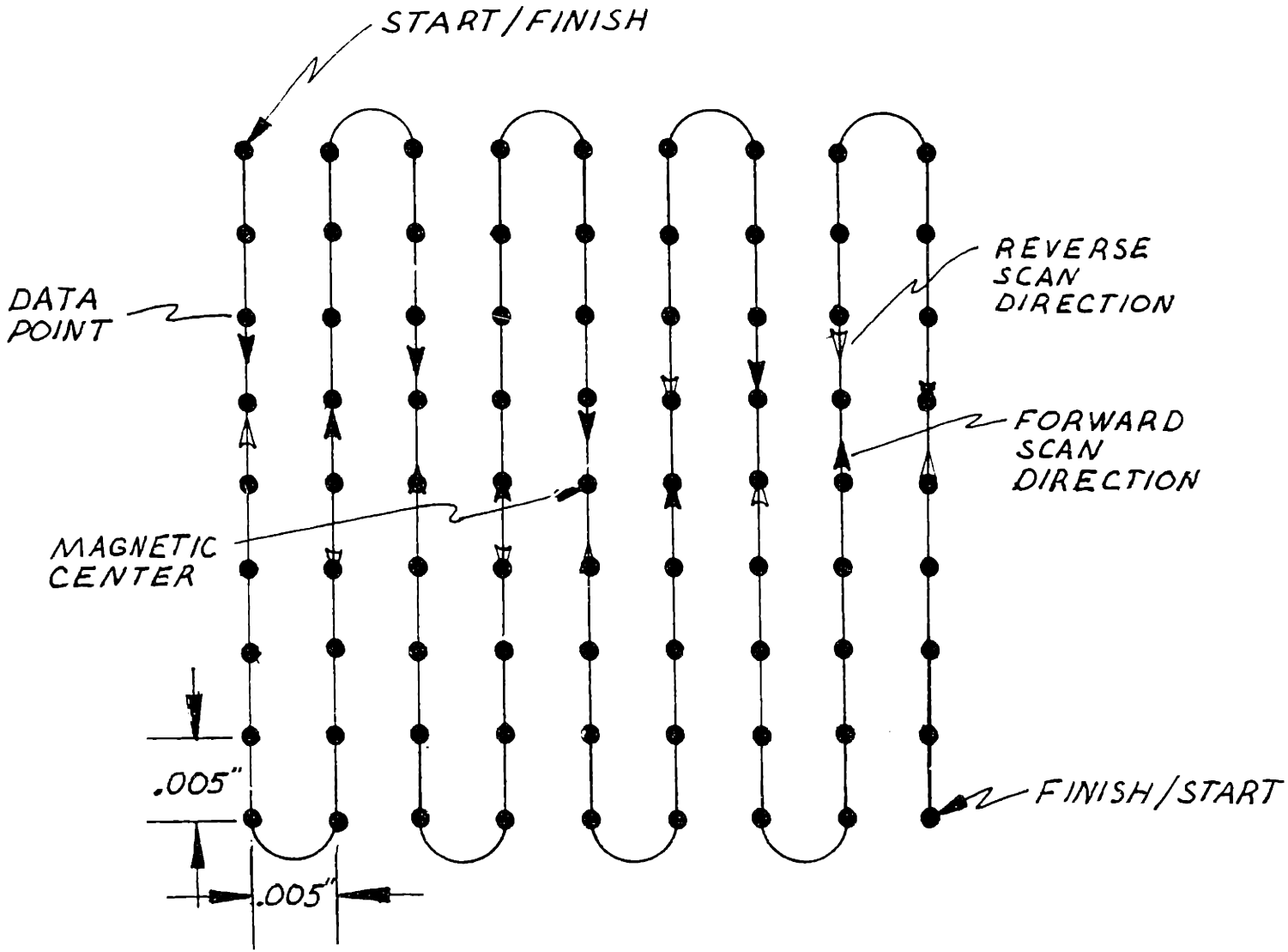

Figure 3.4 - Scan pattern for negative spring constant testing

a) X force

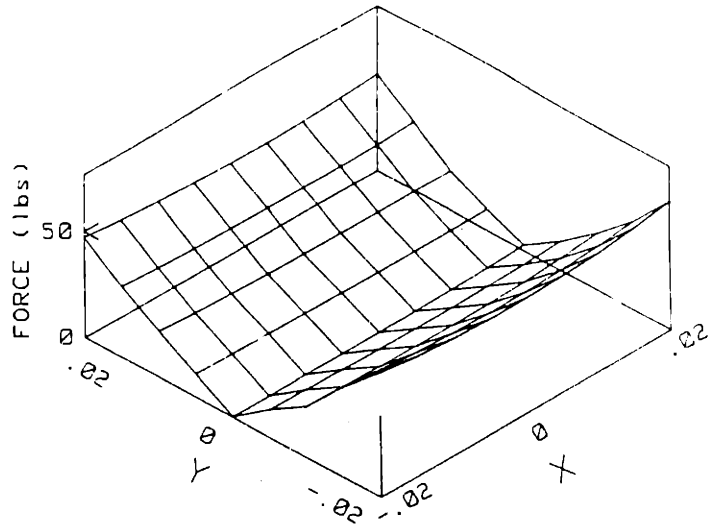

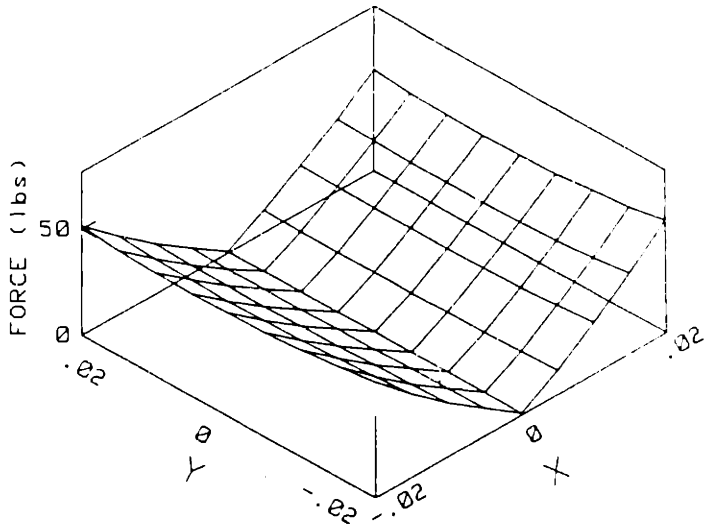

b) Y force

c) Radial Force

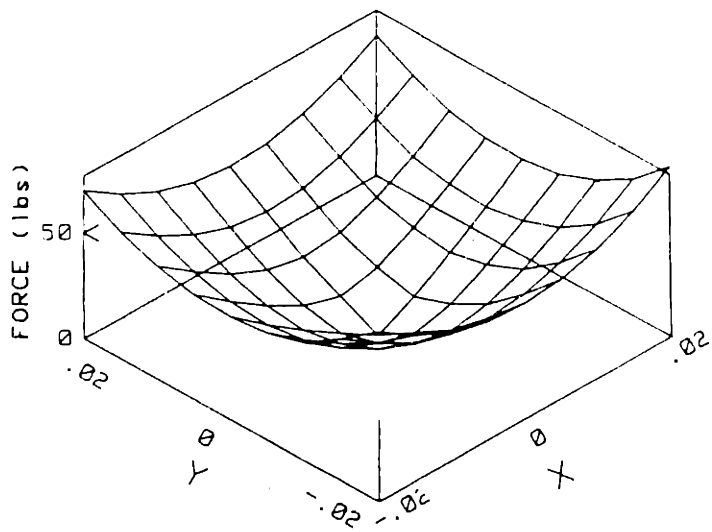

Figure 3.5 - Force vs. position - no current

a) X force

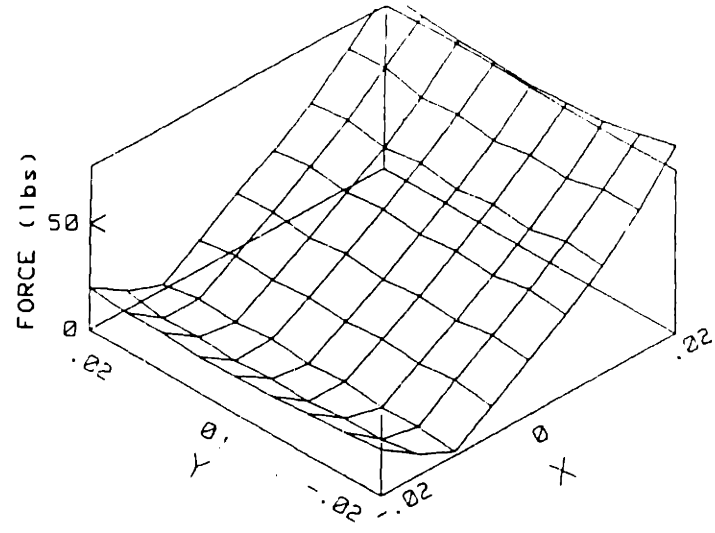

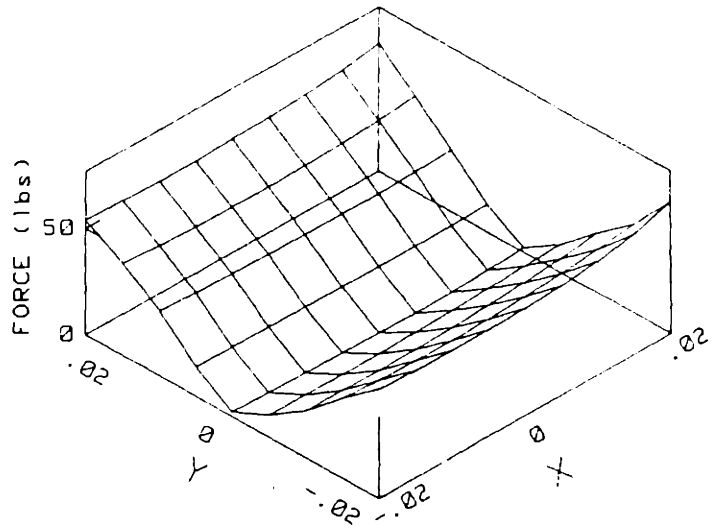

b) Y force

c) Radial Force

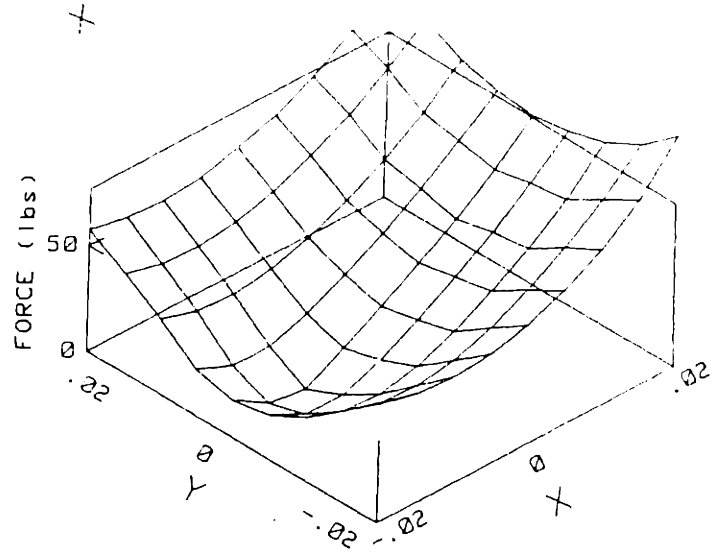

Figure 3.6 - Force vs. position - .2 amps X current

a) X force

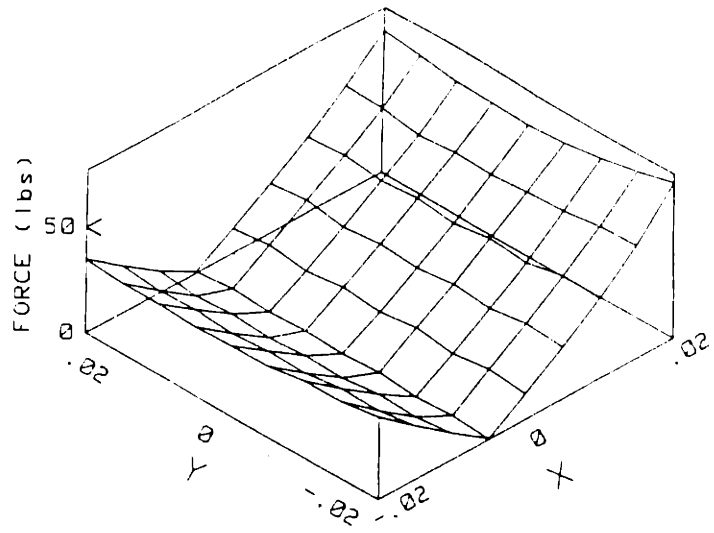

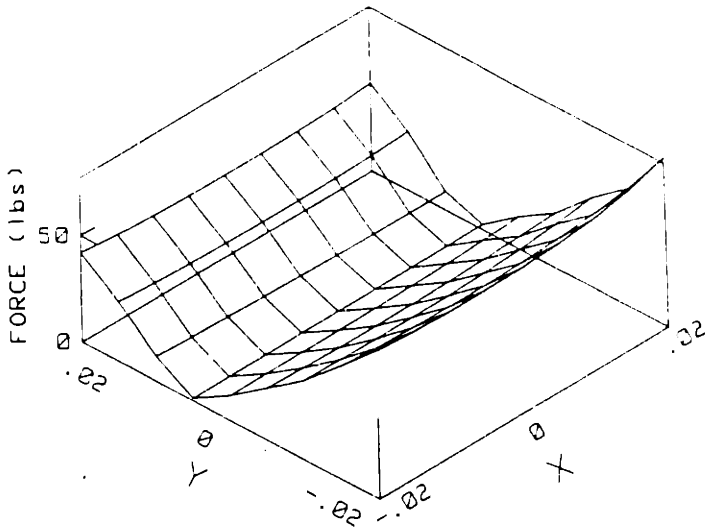

b) Y force

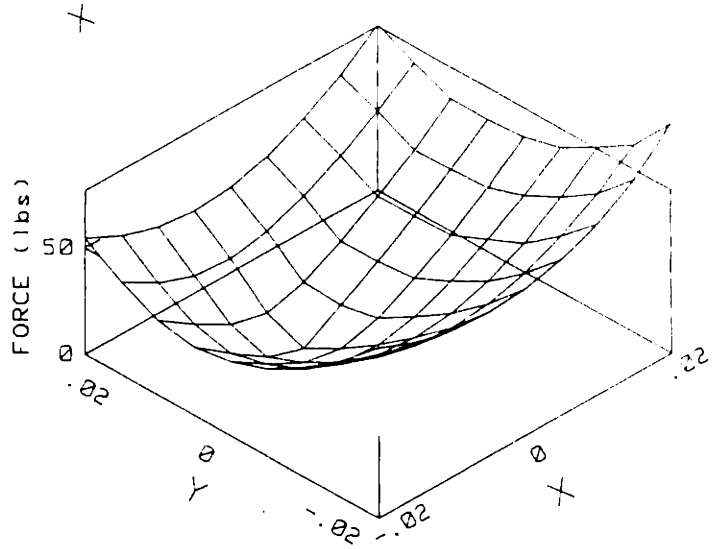

c) Radial Force

Figure 3.7 - Force vs. position - .1 amps X and Y current

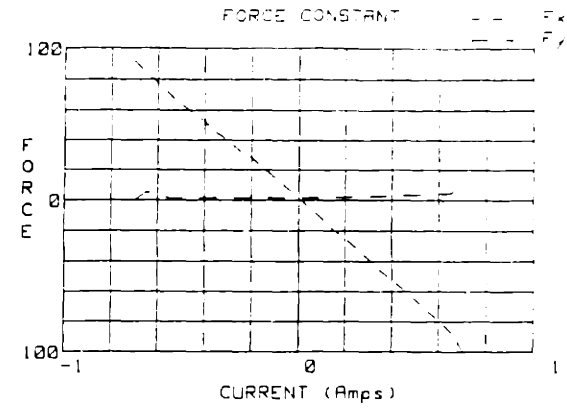

a) Shaft at magnetic center

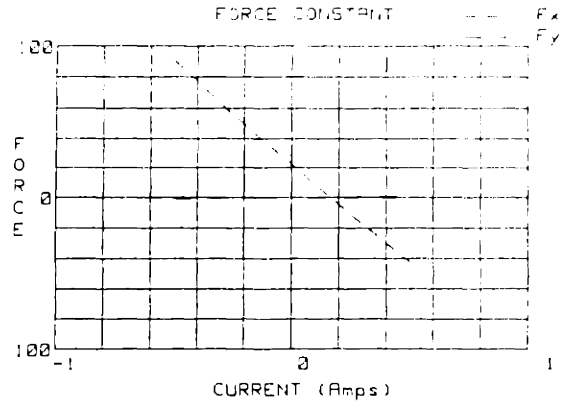

b) Shaft displaced 0.010" on X

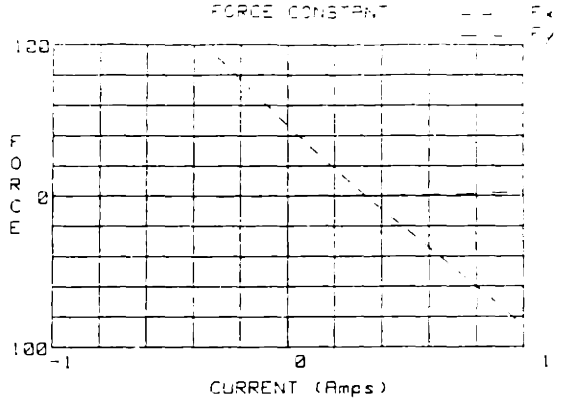

c) Shaft displaced 0.020" on X

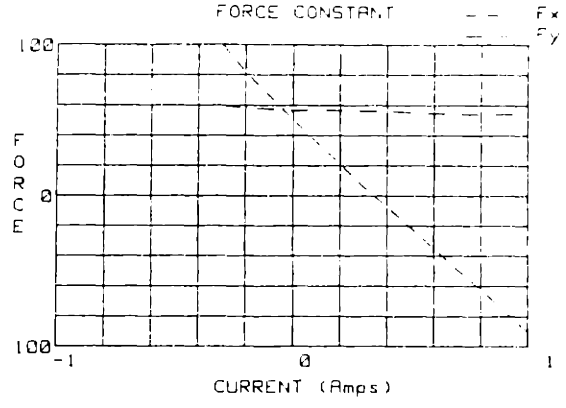

d) Shaft displaced 0.020" on X and Y

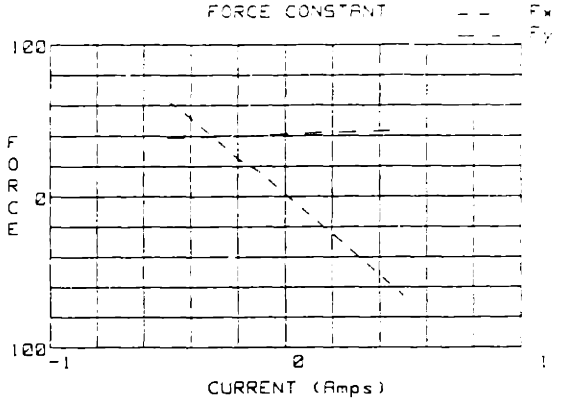

e) .5 amp Y axis cross current

Figure 3.8 - Force vs. current

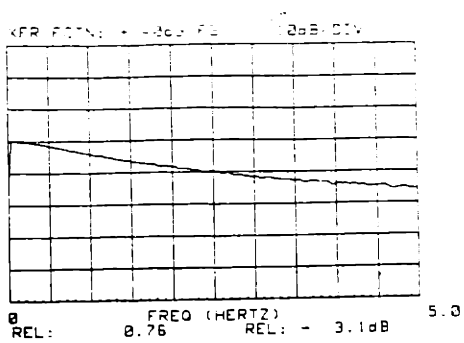

a: Amplitude vs. frequency

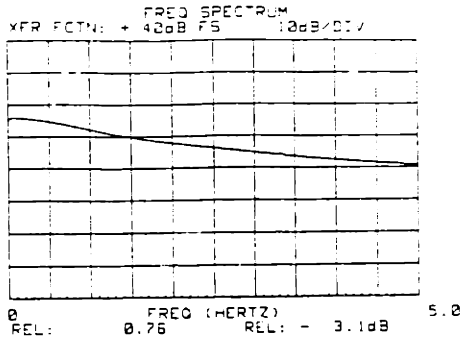

a Amplitude vs frequency

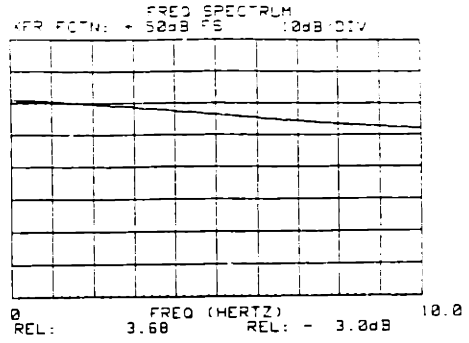

a Amplitude vs. frequency

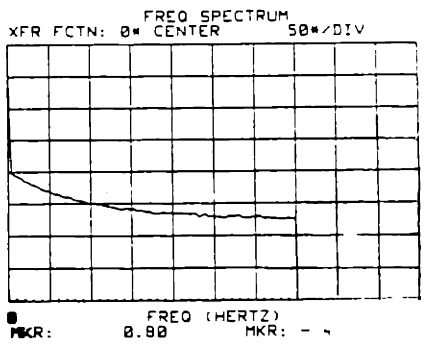

b: Phase vs. frequency

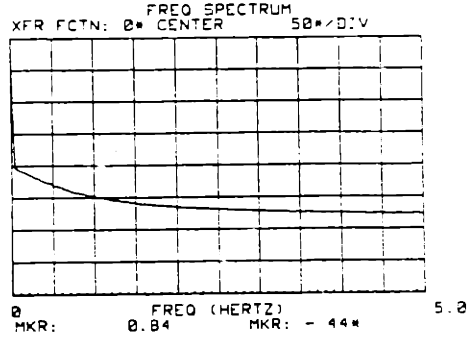

b Phase vs frequency

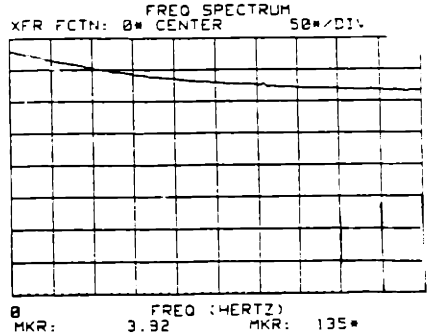

b Phase vs. frequency

a) 80% windings in series

b) 80% windings in parallel

c) 20% windings in series

Figure 3.9 - Voltage to force transfer function

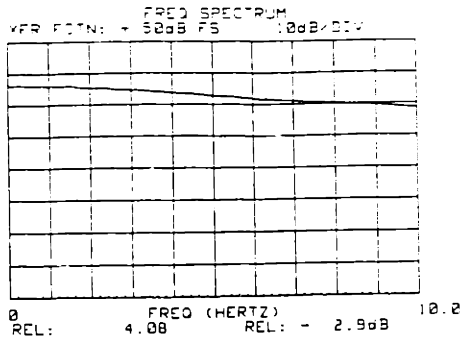

a: Amplitude vs. frequency

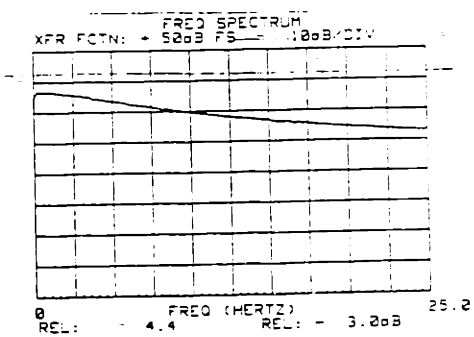

b: Phase vs. frequency

d) 20% windings in parallel

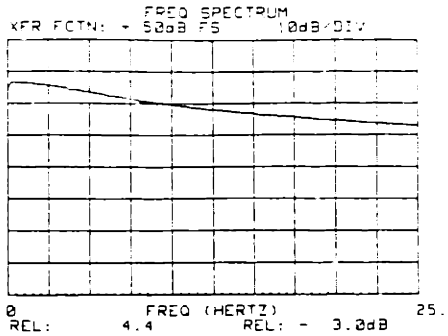

a: Amplitude vs. frequency

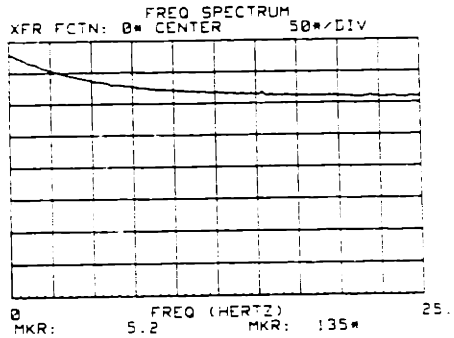

b: Phase vs. frequency

e) 20% winding, single coil

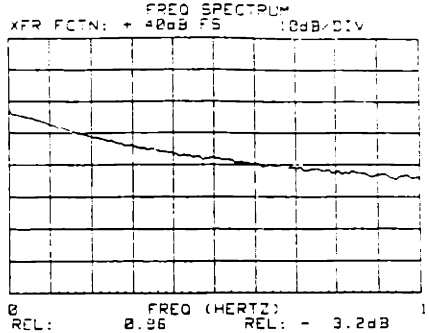

a: Amplitude vs. frequency

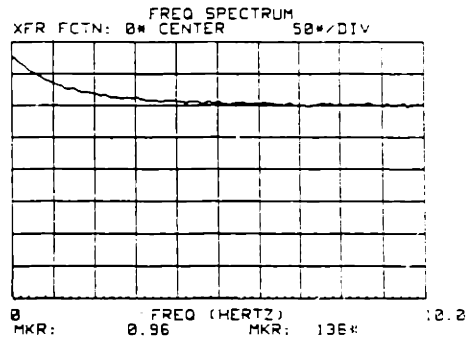

b: Phase vs. frequency

f) 80% winding, single coil

Figure 3.10 - Voltage to force transfer function (cont.)

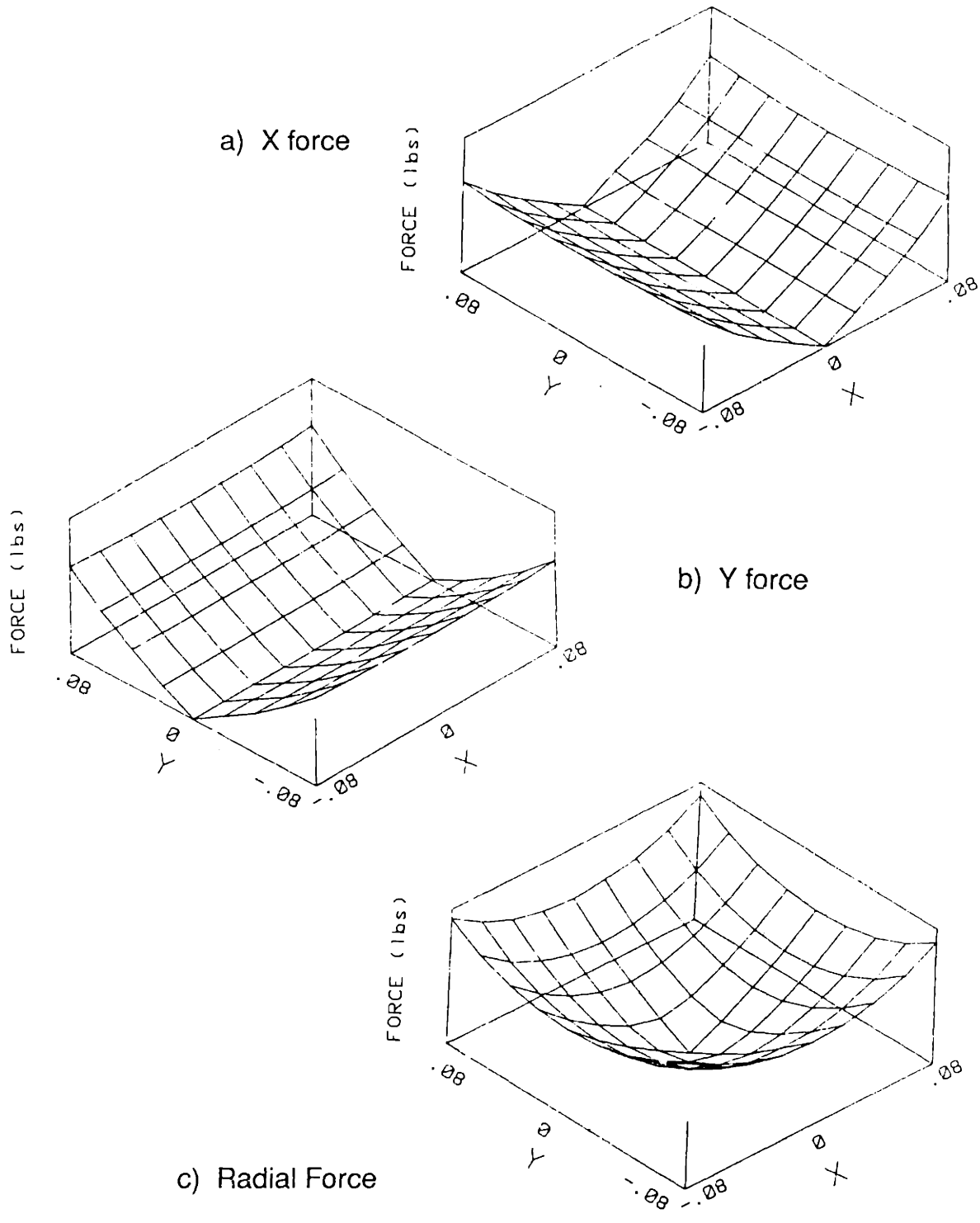

Figure 3.11 - Force vs. position - no current, large gap

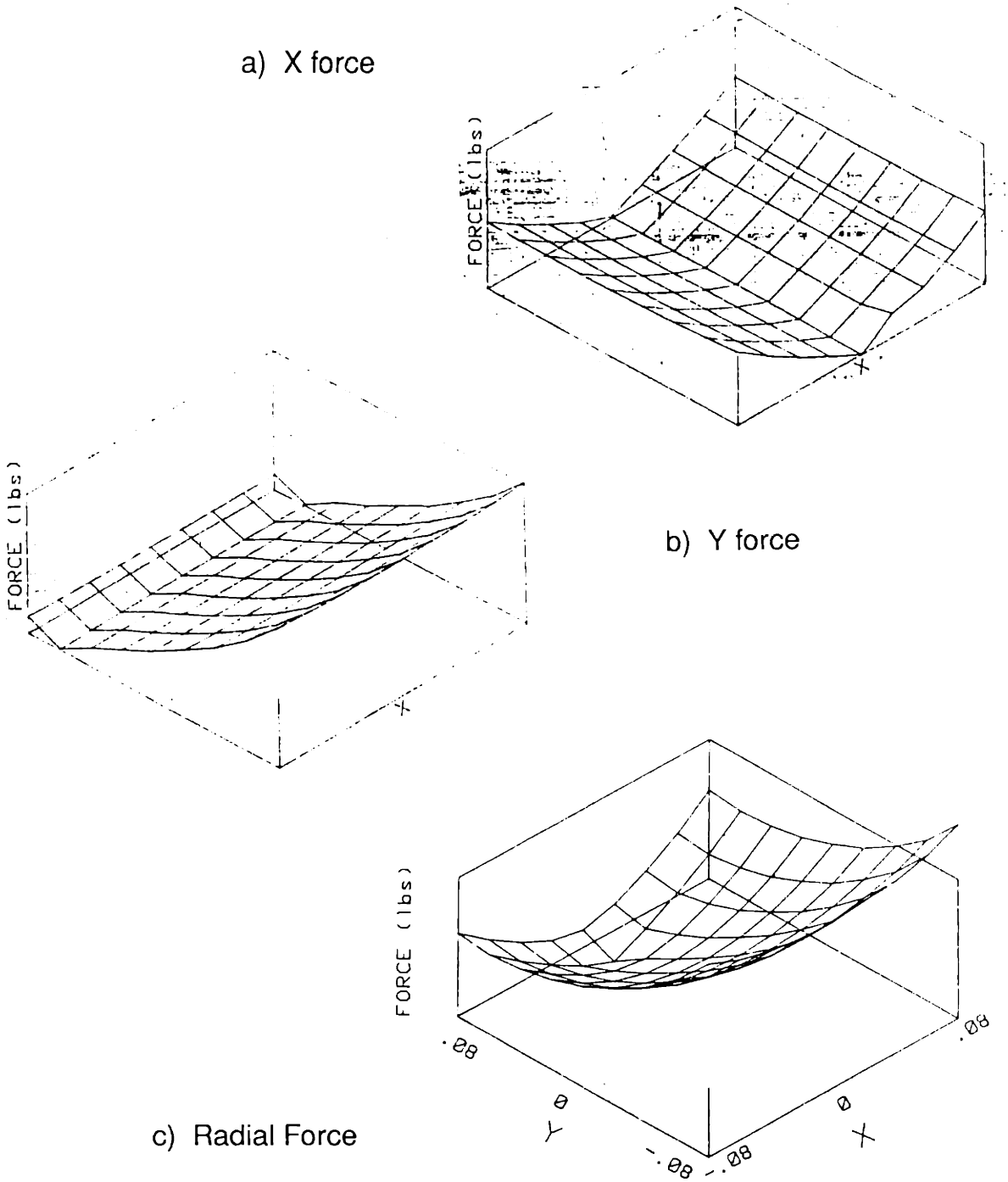

Figure 3.12 - Force vs. position - .4 amps Y current, large gap

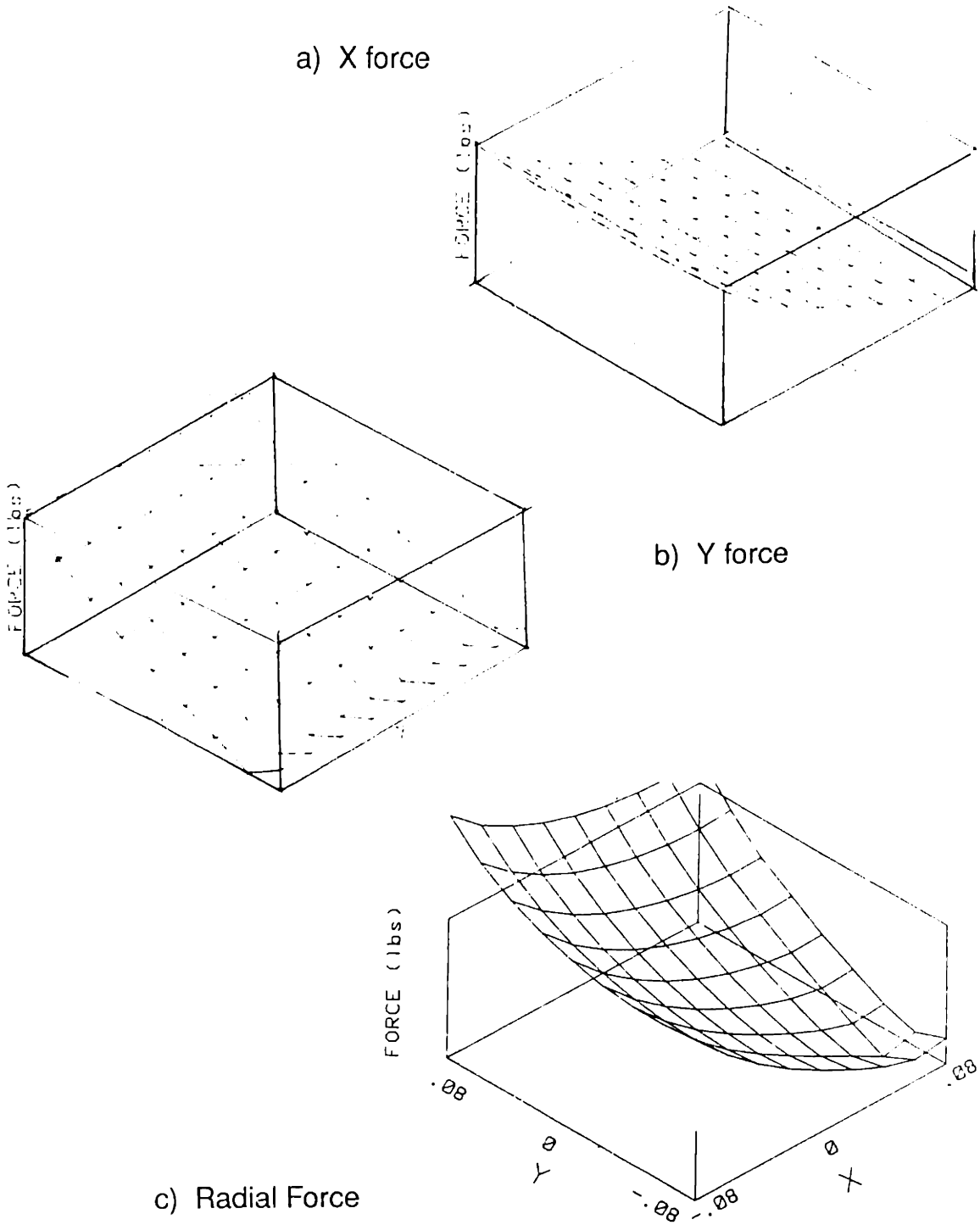

Figure 3.13 - Force vs. position - .4 amps X and Y current, large gap

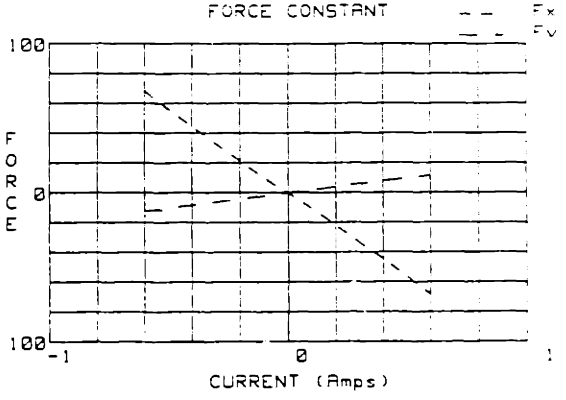

a) Shaft at magnetic center

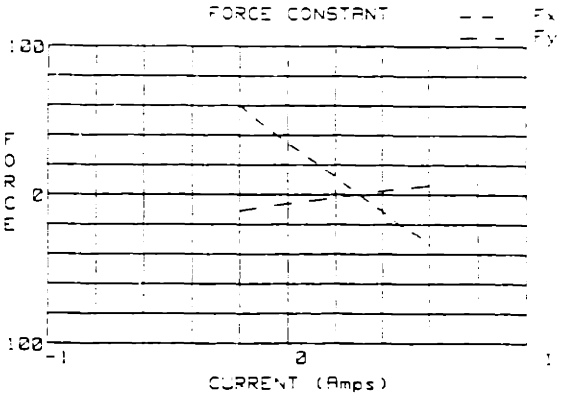

b) 0.050" X displacement

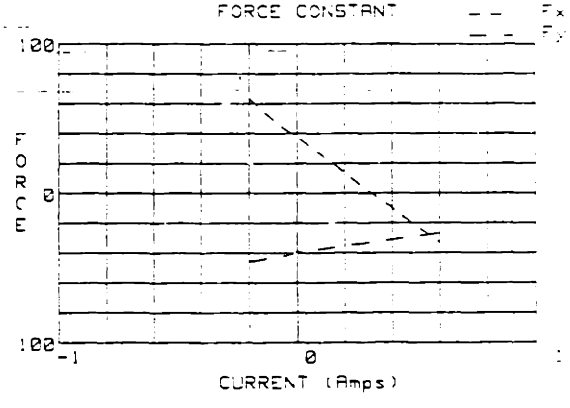

c) 0.050" X and Y displacement

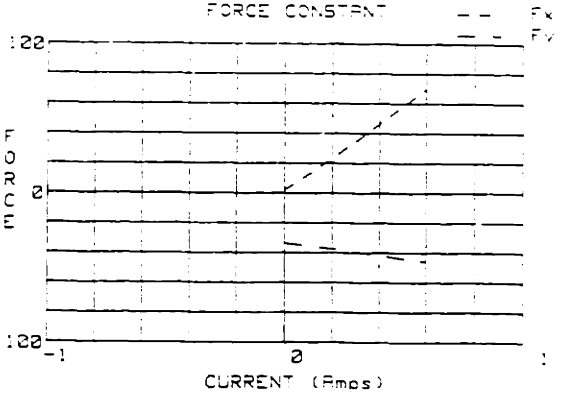

d) 0.050" Y displacement

Figure 3.14 - Force vs. current - large gap

Chapter 4: Single Axis Testing

In addition to the two axis testing, single axis tests were run to check the accuracy of the constants determined in the two axis tests. The servo system is partly based on cancelling the negative spring constant of the bearing with a positive spring characteristic. Accurate force and negative spring constant values are needed to set the controller gains to obtain optimum performance. Single axis testing is better suited for measuring these constants with respect to absolute accuracy, however it ignores cross coupling effects.

4.1 Test Setup

The single axis test rig, shown in figure 4.1, was substantially more rugged than the two axis rig. This is mostly because large (and hence very stiff) load cells were available. Also their single axis nature allowed a heavier rig design to hold the bearing. The rig consisted of a mounting fixture that held the bearing, which was mounted on two ball slides. Two load cells transduce force between the fixture and ground. The shaft target was attached to ground. Since the load cells were designed for compression only, the two are loaded against each other, and the difference between the two is the force being exerted on the core. Two micrometer heads position the bearing by pushing on the two load cells. These heads are also used to preload the cells against each other. A differential amplifier processes the load cell outputs

and gives a voltage output proportional to the total force. A "Federal Gauge" displacement transducer is used to measure the actual bearing movement.

This rig is more accurate than the two axis rig for several reasons. First the bearing travels on a slide and cannot tilt, thus eliminating tilt error. Also, the shaft is far stiffer than the two axis rig, and thus errors induced by its deflection and tilting will be eliminated. The nature of the load cells also improves the system accuracy. Since these are one axis load cells, there is no cross coupling to induce error. These load cells can also be calibrated with a precision weight, whereas the two axis load cell had to be calibrated with a force gauge (basically another load cell). The one axis load cells did exhibit hysteresis, however. This was cancelled out by taking measurements in two directions and averaging the results, as was done in the two axis testing. The result is that the force and negative spring constants can be determined reliably to at least three significant digits. In the two axis tests they are good to two significant digits at best.

4.2 Static Testing

Although the single axis testing is more accurate, it only determines the on-axis constant values, but not their dependence on the other axis' inputs. However, the tests are essentially the same as their two axis counterparts. In the negative spring constant test the core is moved within the gap and force is measured at several

positions. The measured negative spring constant was 1,550 lbs/in. This is quite a bit lower than the two axis number of ≈2,500 lbs/in.

The force constant test measures force at a variety of different coil currents. There were two force contants measured, one for the large coils (80% windings) and one for the small coils (20% windings). Both are for the case in which the coils are driven in parallel. They are 53.1 lbs/amp and 14.1 lbs/amp, respectively. When the coils are driven in series, the force constant should be twice the parallel value, since the coils will use the same current instead of splitting it. To check this the 20% windings were tested in series. They force constant in this configuration was 27.4 lbs/amp, roughly twice the parallel value. The two axis tests measured 135 lbs/in for the 80% windings driven in series.

The constant values measured are substantially higher in the two axis tests than in the single axis tests. There are several possible explanations for this. In the two axis testing the shaft that held the core and the load cell were substantially less stiff. Thus the shaft could have tilted several degrees relative to the bearing pole face when the force got large. This would make the gap smaller and thus the force greater as compared to the case in which the core is exactly parallel to the pole face. The the force and negative spring constants would seem larger than they really are. Another possible explanation is temperature. The two sets of test were conducted in different locations, and there may have been a temperature difference. The magnetic properties of materials are

very temperature sensitive, and may have contibuted to the discrepancy. Temperature probably couldn't cause all of the discrepancy, however. It is doubtful that the discrepancy was caused by a load cell calibration or cross coupling error, as these were checked and found to be much smaller than the difference in constant values. (see sect. 3.4).

4.3 Dynamic Testing

Coil current to voltage transfer functions were also measured on the single axis test rig. A transfer function analyzer and an HP computer to support it were available. The transfer function analyzer measures the current and voltage of the bearing at discrete frequencies, as opposed to using white noise, which the spectrum analyzer used. Although these methods produce the same results, the discrete frequency method gives a cleaner transfer function over a wider frequency range. Plots of the various coils in both series and parallel arrangements are shown in figures 4.2 through 4.4. The inductances calculated from these curves are listed in table 4.1. They compare quite well with the inductances determined from the testing done in the two axis test rig. The test apparatus stiffness is not important in the dynamic testing, as only current and voltage are being observed, and not force.

Inductance measurements were also made with an inductance bridge while the bearing was in the single axis test rig. The inductance bridge is a device that drives the coils at a high

frequency (in this case 2000 Hz) and balances its with impedance with a calibrated impedance. These measurements are very similar to the inductances measured via reactance in the two axis testing. Likewise they have the same shortcomings, in that they are not a true inductance measurement. (see sect 3.5.6) The bridge measurements are also listed in table 4.1

Table 4.1: Small gap inductances, as determined from voltage/current transfer function and inductance bridge

Coils	Config.	Break Freq (Hz)	L (mH)	L-Ind. Br. (mH)
80%	series	1.0	993	545
80%	parallel	1.0	248	163
20%	series	4.4	58	11
20%	parallel	4.4	15	33

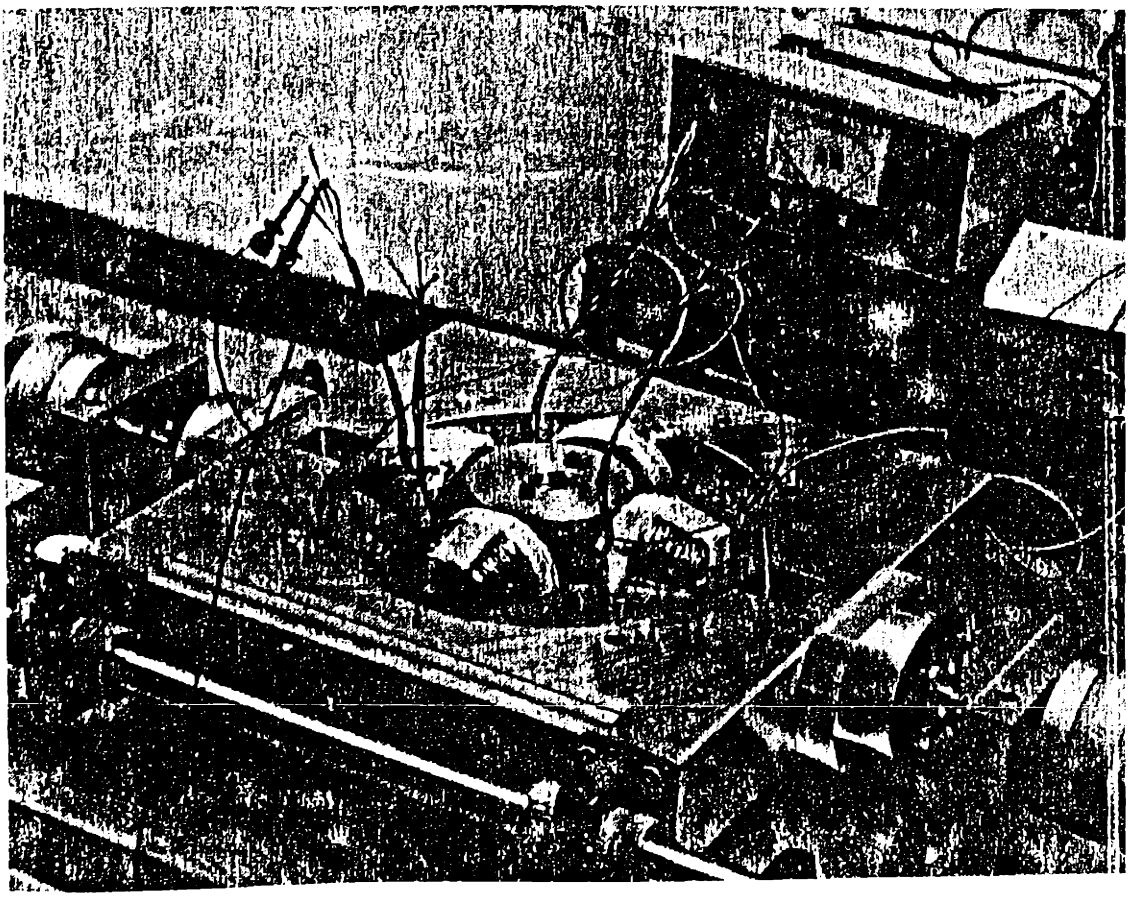

Figure 4.1 - Single axis test apparatus

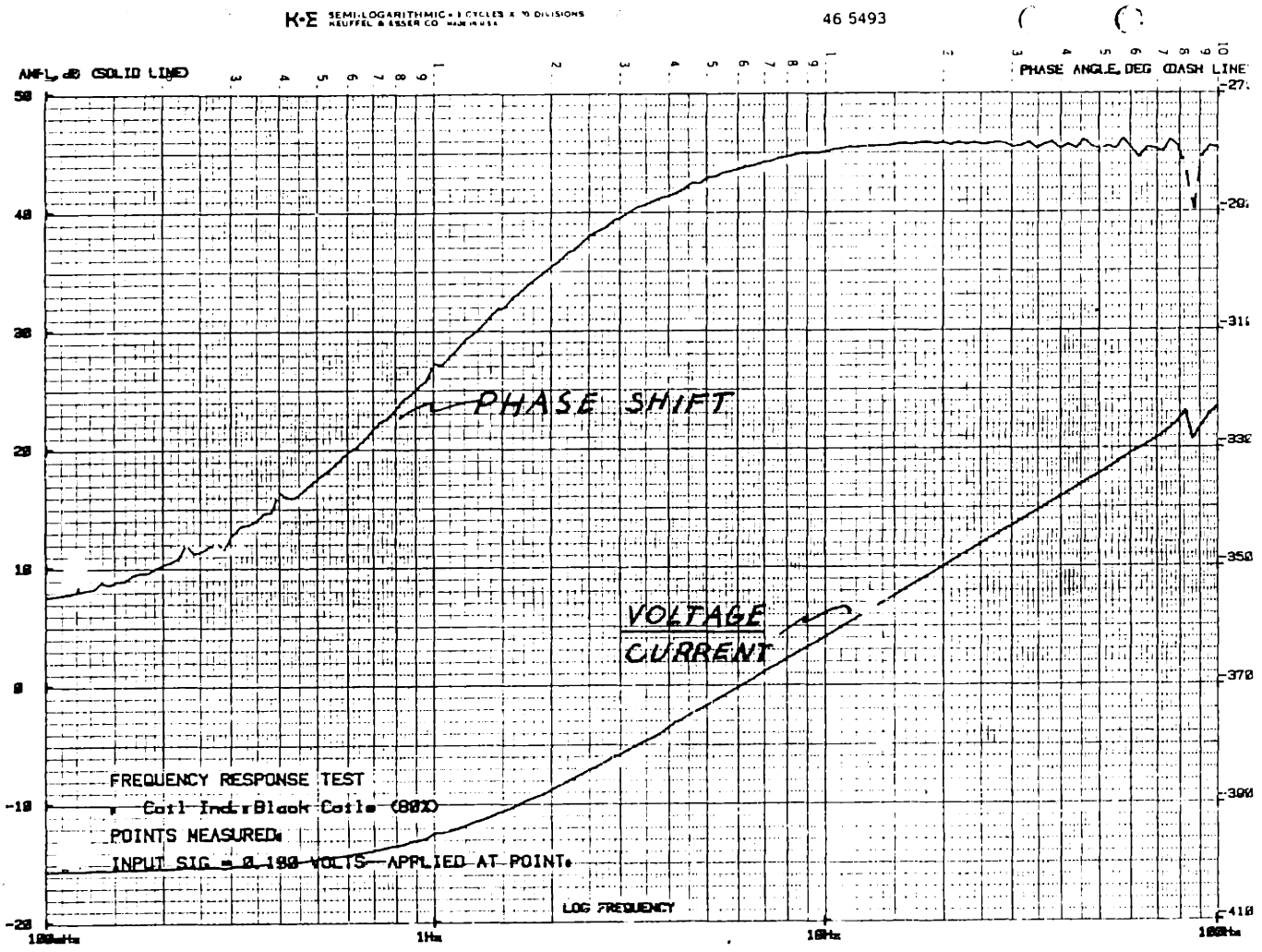

Figure 4.2 - Frequency response of 80% windings - series configuration

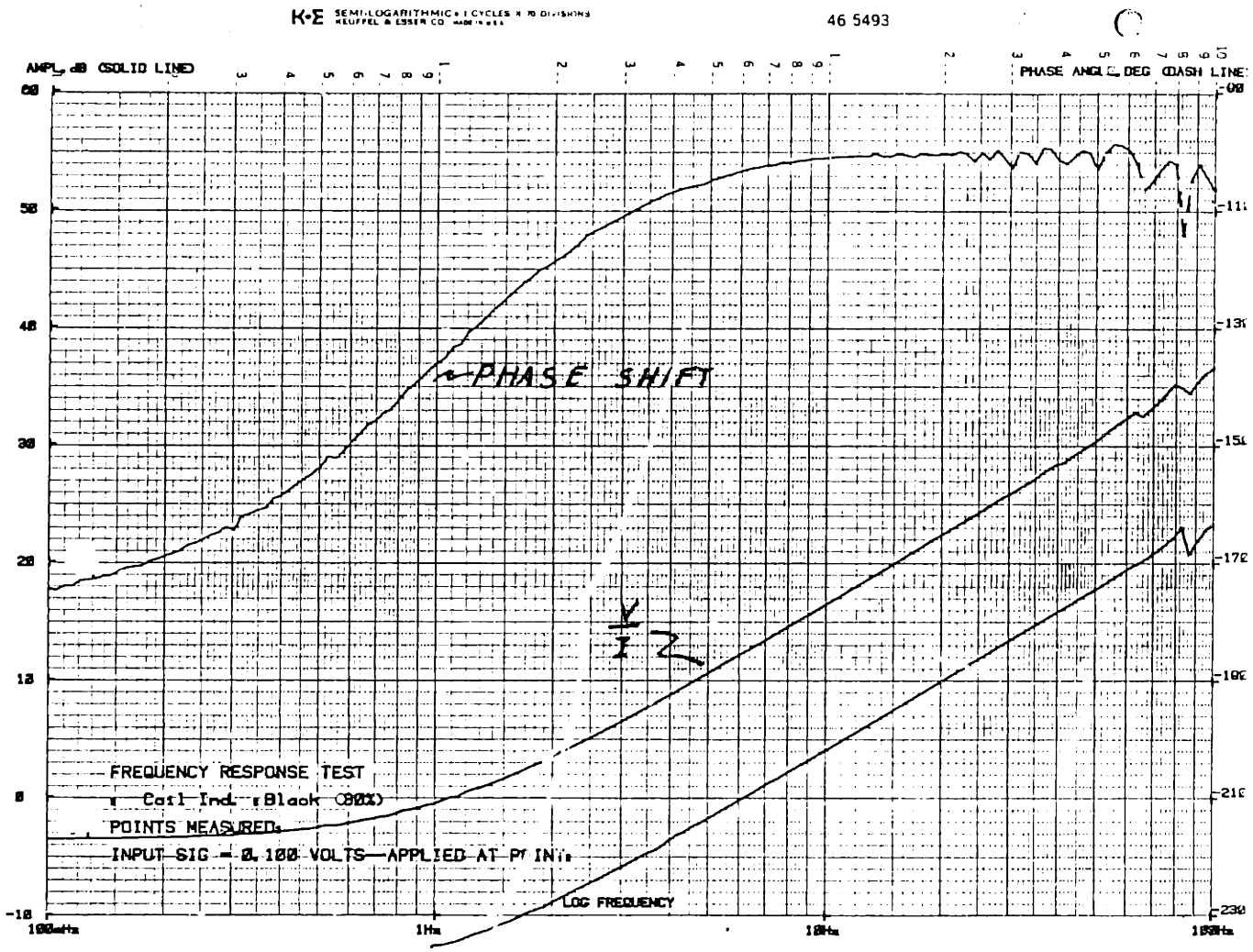

Figure 4.3 - Frequency response of 80% windings - parallel configuration

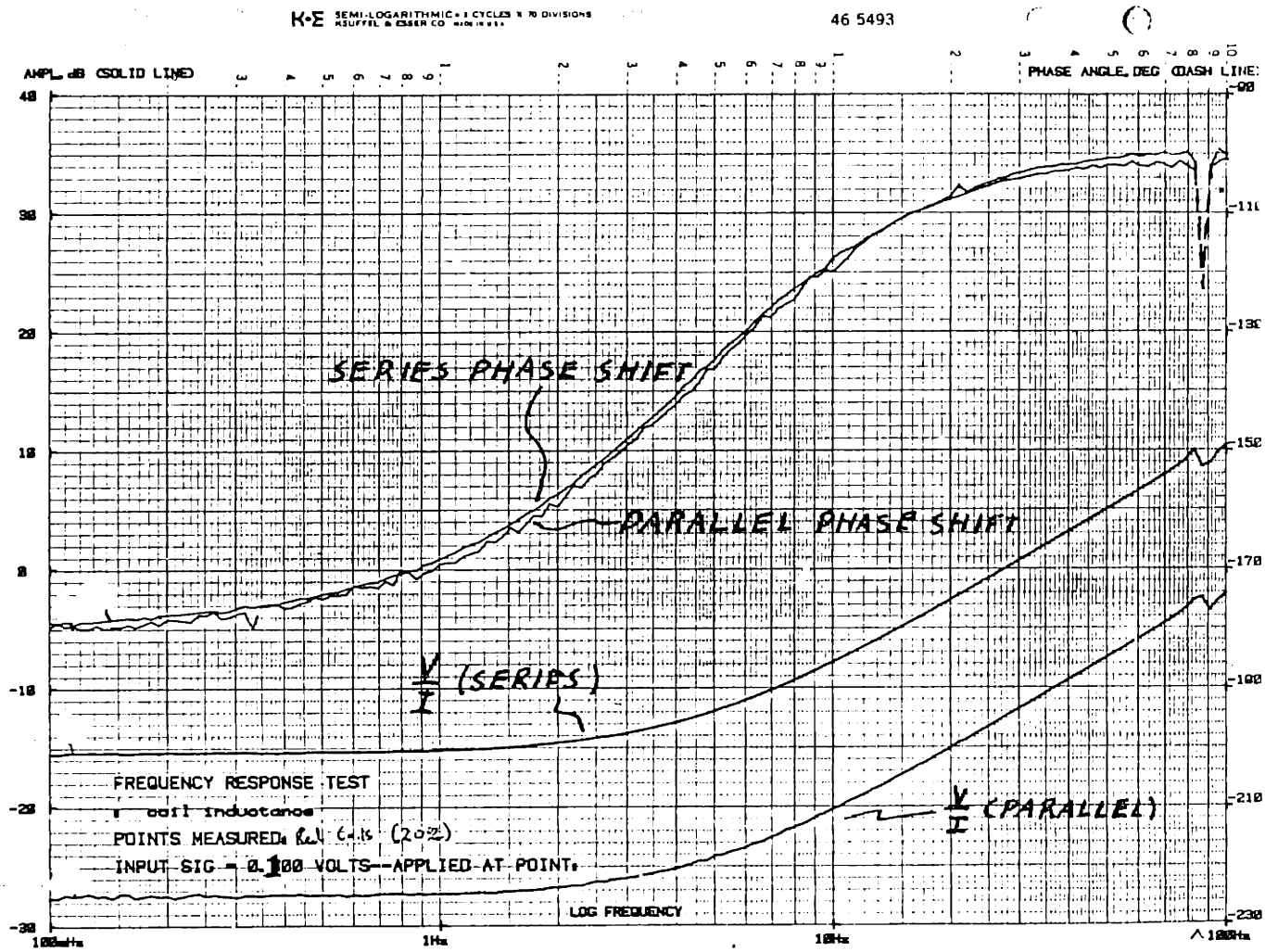

Figure 4.4 - Frequency response of 20% windings - series and parallel configurations

Chaper 5: Finite Element Analysis

In order to analyze two dimensional phenomena of the magnetic bearing, such as cross coupling, a two dimensional analysis tool is needed. Because two dimensional analysis is beyond the capabilities of most manual calculations, computer methods are best suited to this task. MAGGIE, a magnetic finite element program developed by the A.O. Smith Company, performed the magnetic bearing two dimensional analysis on an IBM PC.

The first step in the analysis is the creation of a finite element mcdel of the device. The model consists of the device broken up into many small triangle elements. Each triangle's coordinates, material properties, and boundary conditions are entered into the computer. The computer creates a large matrix of all of the elements, and solves it for the desired output variables. In this case, given the magnet strengths and coil currents, it solves for the magnetic vector potential and flux density. With this solution, a complete magnetic picture of the device can be obtained. Two forms of data are created. First, the program generates a table of flux densities in each element and vector potentials at each grid point. This table is useful in determining the flux in crucial areas, such as air gaps, so that items such as force can be calculated. Also, by piecing together the flux densities and the vector potentials over the whole model, the program generates a plot of the flux lines in the device. The flux plot is valuable for identifying

areas of magnetic saturation and leakage. This is a very powerful tool that gives information otherwise not available through one dimensional analysis.

In the case of the PFC magnetic bearing, a finite element model was created with 704 elements and 380 grid points connecting them. The model used a linear model of the Samarium-Cobalt magnets as well as a linear model of the back iron. Table 5.1 lists the material input parameters. This model is shown in figure 5.1.a. Figure 5.1.b shows a detail of the gap in the model. The gap area was broken into smaller triangles than the rest of the bearing to provide more accurate modeling in this crucial part of the bearing. A large gap model was also constructed, shown in figure 5.2 The gaps on the exterior ring of this model are the magnet positions. They were omitted in this diagram for clarity.

Table5.1: Finite Element Model Material Inputs

Material:	Air	$\mu_r = 1$
	Steel	$\mu_r = 4000$
	Magnet	$\mu_r = 1.1$
		$H_C = 716{,}000$ Oersteds
	Coils	$\mu_r = 1$
		700 turns per coil

For each different test point, a new model had to be run. Thus every individual displacement and every individual current had a separate model and a seperate run associalted with it. A total of 36 different models of the PFC bearing were run. Basically, a model of a particular shaft displacement was run at several currents (including zero amps). Models were constructed for single axis displacements of 0, 0.010", 0.020", and 0.040". A model of 0.020" X and 0.020" Y combined displacement was alsc run, in order find the cross coupling. All of the above models were run at 0, 0.50, and 1.0 amps current. Models were run with both large and small gap configurations. A series of models with varied magnet strength was also run.

The MAGGIE results were used primarily to analyzed the negative spring and force constants of the bearing. These numbers were obtained by looking at the bearing forces at various displacements and currents, much like the actual testing. The bearing forces were obtained by finding the flux in the gaps from the flux density tables given in the output. The flux density is averaged over all the gap elements. The force proportional to the average flux density squared, as given in equation (2.3):

$$F = \frac{\beta^2 A}{2\mu_0} \qquad (1)$$

where B is the flux density, A is the pole area, and μ is the permeability of free space. Using this equation, all the gap forces

can be calculated, and hence the resultant force on the core can be determined. The gap forces are always attracting the pole towards the core. It is the difference in these forces that generates the net force on the core.

The first set of runs were for a series of displacements along the bearing's axis. Table 5.2 lists the negative spring and force constants for each displacement. They are substantially higher than any of the constants measured during the tests. Part of the reason for this lies in the nature of the finite element model. MAGGIE is a two dimensional finite element modeler. It assumes the bearing is of inifinite thickness, ie., having no leakage from the top and bottom of the bearing. Since the bearing is quite thin relative to its diameter, there is a significant amount of end leakage that maggie doesn't model. The program does model the in-plane leakage, that is, the leakage between the poles and out of the circumference of the bearing.

Table5.2: Bearing Constants from Finite Element Analysis

Displacement	-Kx (lb/in.)	Kf (lb/amp.)
.000"	-	177
.010	5,531	181
.020	5,716	188
.040	6,578	229

Runs were made with both simultaneous X and Y displacement, and simultaneous X and Y currents in order to investigate the model prediction of cross coupling. At 0.020" X and Y displacement,

MAGGIE indicates a negative spring constant 5,915 lbs/in, which is 3.5% above the on axis value of 5,716 lbs/in. An increase of 9.5% was seen in the experimental work. At 0,0 displacement with a .5 amp cross axis current the force constant was 177 lb/amp, which is the same as with no cross axis current. Thus MAGGIE predicts that there is no current cross coupling. The experimental values indicate a 6% decrease in force constant with a .5 amp cross axis current.

Another reason for the program's over estimation of the constants may not even lie in the program itself. Although the bearing's permanent magnets are supposed to be magnetized to a certain specification, they were never measured to check their magnetization. Thus they may not be fully saturated as much as we have assumed. This is not uncommon in Samarium-Cobalt, since it is such a magnetically hard material, and if the magnetizing field is not sufficient, they may not have been fully saturated at manufacture. To investigate how this would effect the bearing's performance, another set of models was run with the magnets of ony 1/2 the cooercive force of the original models. This set of runs indicated a negative spring constant of 1,430 lbs/in and a force constant of 88 lbs/amp. These values are much closer to what was measured during the bearing testing.

Becuase the 1/2 magnet strength runs were closer to what was found in the experimental work for the small gap configuration, large gap analysis was done with the 1/2 strength magnets also. The large gap model predicted a negative spring constant of 103

lbs/in and a force constant of 16 lbs/amp. Table 5.3 compares the constant values from the MAGGIE analysis to what was measured in the tests. The small gap figures are from the single axis testing, whereas the larg gap figures are from the two-axis testing. The MAGGIE figures are from the 1/2 strength magnet runs. The MAGGIE values are consistently below those of the experimental testing, which indicates that a factor of 2 was more than was needed in the reduction of the magnet's cooercive force. Obviously the cooercive force could be "tuned" to match the experimental values, making the absolute matching meaningless. However the relative values appear to be consistent, and if the coercive force of the magnets were known, MAGGIE results would most likely match the experimental data.

The flux density data helps to substantiate this claim. The change in flux density in the gaps is independent of the magnet strength, and depends solely on the coil currents. For the small gap configuration, MAGGIE predicts a change in flux density of .48 tesla for a 2.0 amp coil current. The experimental values are between .48 and .54 tesla. In the large gap case MAGGIE indicates a .065 tesla change in flux density, where a .058 tesla value was obtained experimentally. The good match in this data indcates that the end leakage was not that significant, and that the improper magnet strength caused the exterme mismatch between MAGGIE and experimental data.

Table5.3: Comparison of Bearing Constants Between Finite Element Analysis and Experimental Values

	Force Const.		Neg. Spg. Const.	
Gap Config.	Exp.	MAGGIE	Exp.	MAGGIE
Large	25	16	153	103
Small	103	88	1550	1430

As mentioned above, MAGGIE also gives flux plot output as well as flux density tables. The flux plot for the no displacement, no current case is shown in figure 5.3. The plot shows the four permanent magnet circuits, which run around each quadrant of the bearing. The gap detail shows that the flux density is fairly uniform throughout the gap. There is some slight fringing on the edges. This also shows in the flux density data. Figure 5.4 shows the flux plot for the case where the permanent magnets have been replaced with air and two opposing coils are driven. This is the electromagnet magnetic circuit. There are two which run through halves of the bearing. The gap detail shows that there is no flux flowing across the non-driven gaps. Thus there is no change in flux density in the cross axis, and no cross axis force. A flux plot from driving a single coil is shown in figure 5.5. Here most of the flux travels through the side gaps, but some travels through the opposite gap. This is an indication of the inductive coupling between two opposing coils. The inductance data indicates that the coils are partly coupled. The flux traveling through the opposite pole substantiates this.

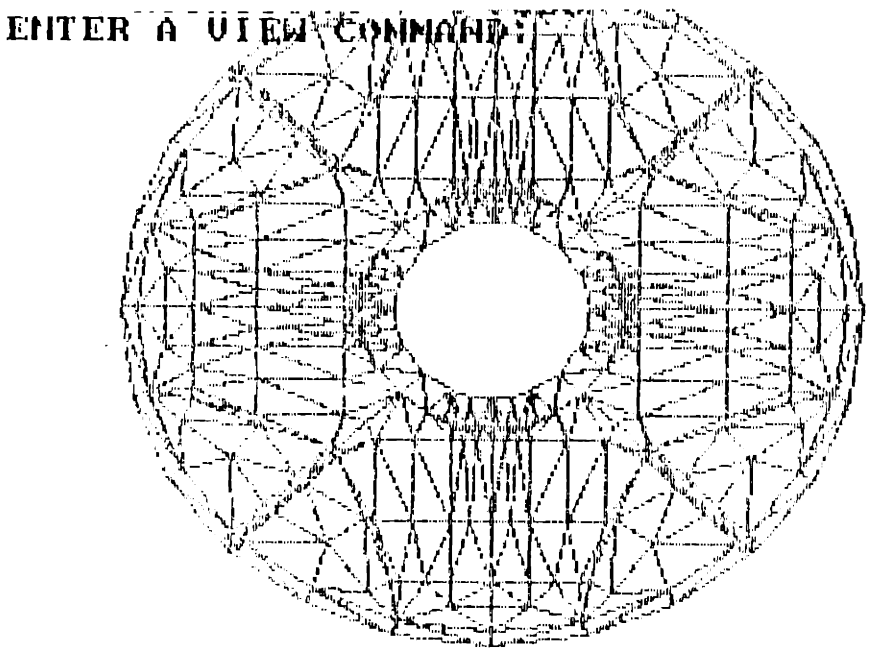

Figure 5.1a - Small gap finite element model

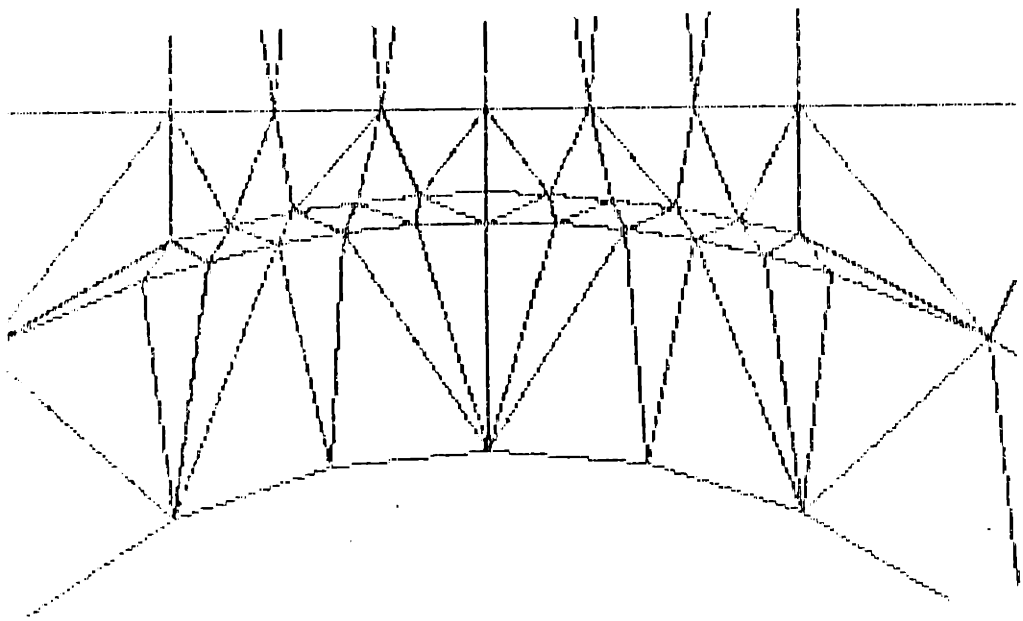

Figure 5.1 b - Gap detail of small gap model

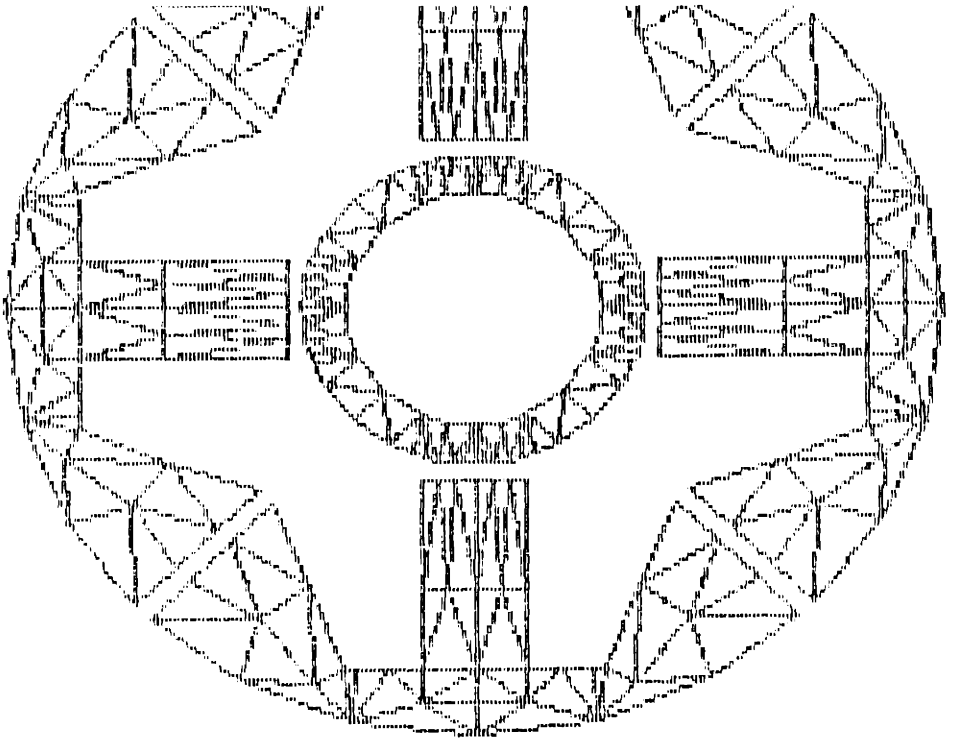

Figure 5.2 a - Large gap finite element model - magnet and air elements not shown

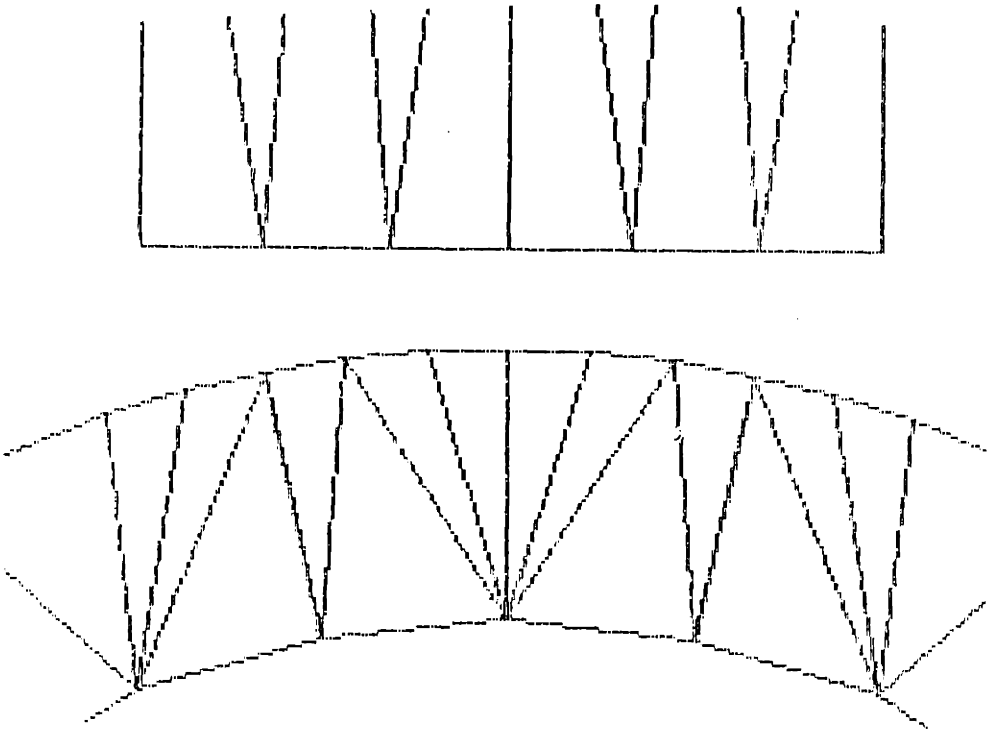

Figure 5.2 b - Gap detail of large gap model

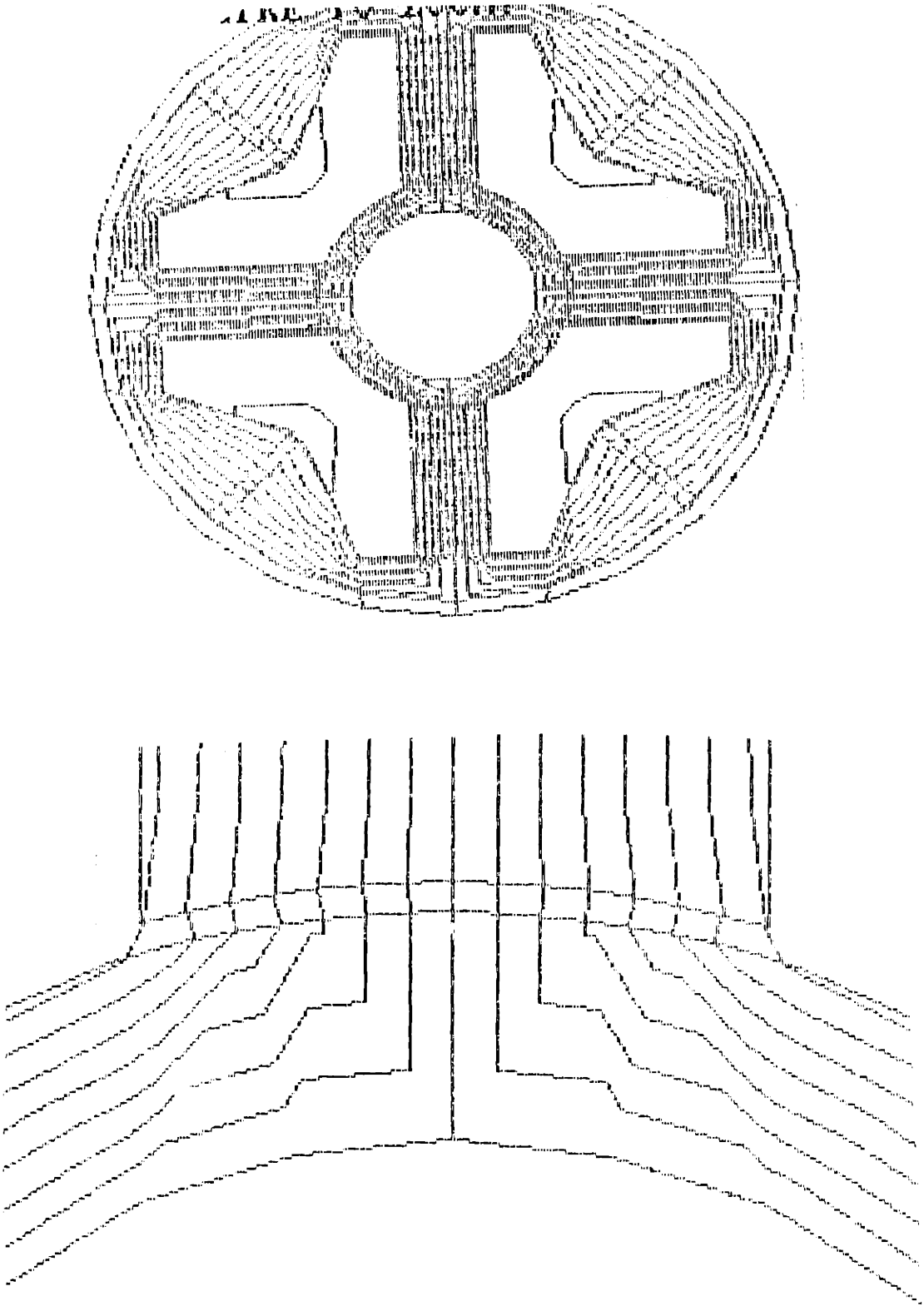

Figure 5.3 - Flux plot, no displacement, no current case

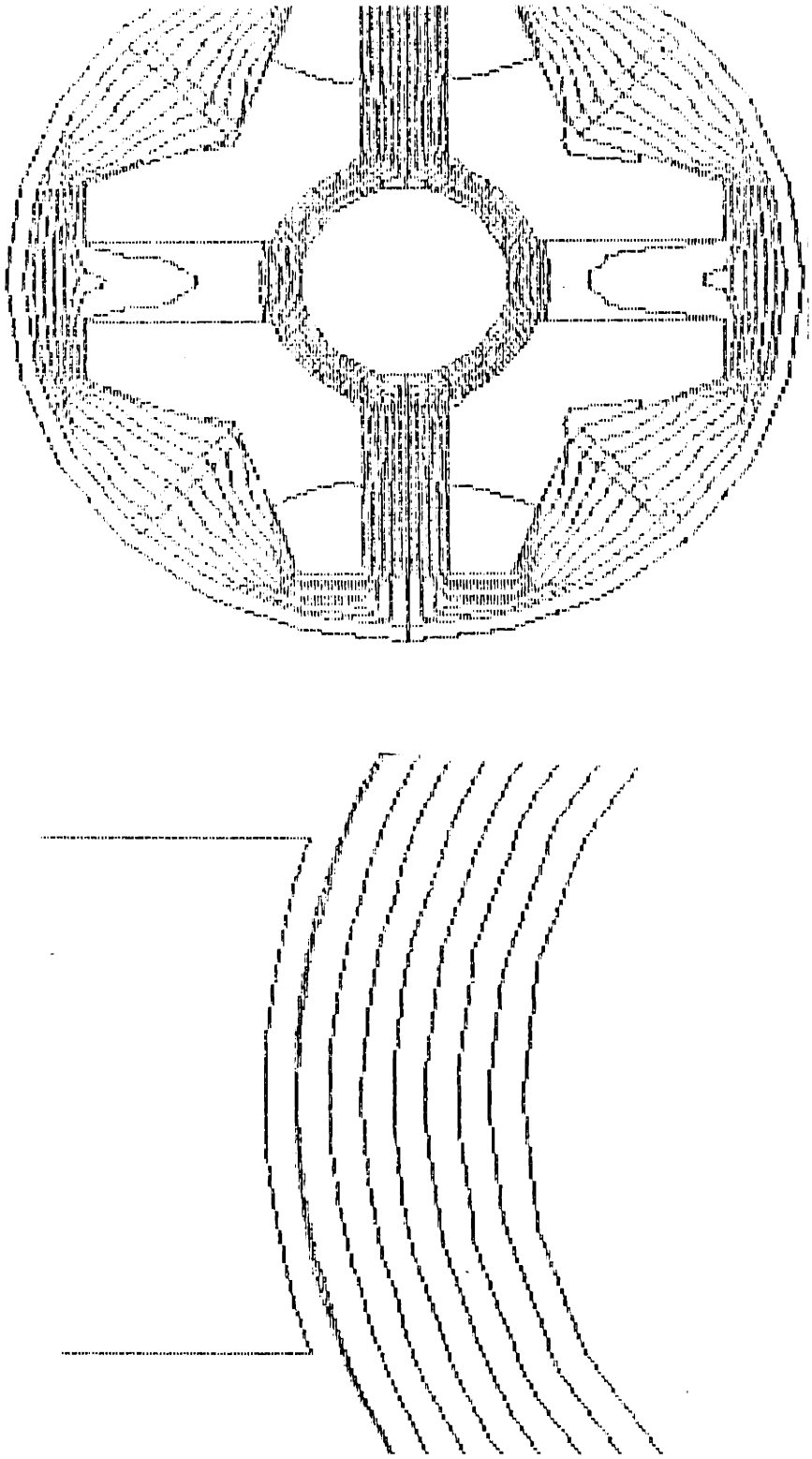

Figure 5.4 - Flux plot, Two coils driven, no permanent magnets

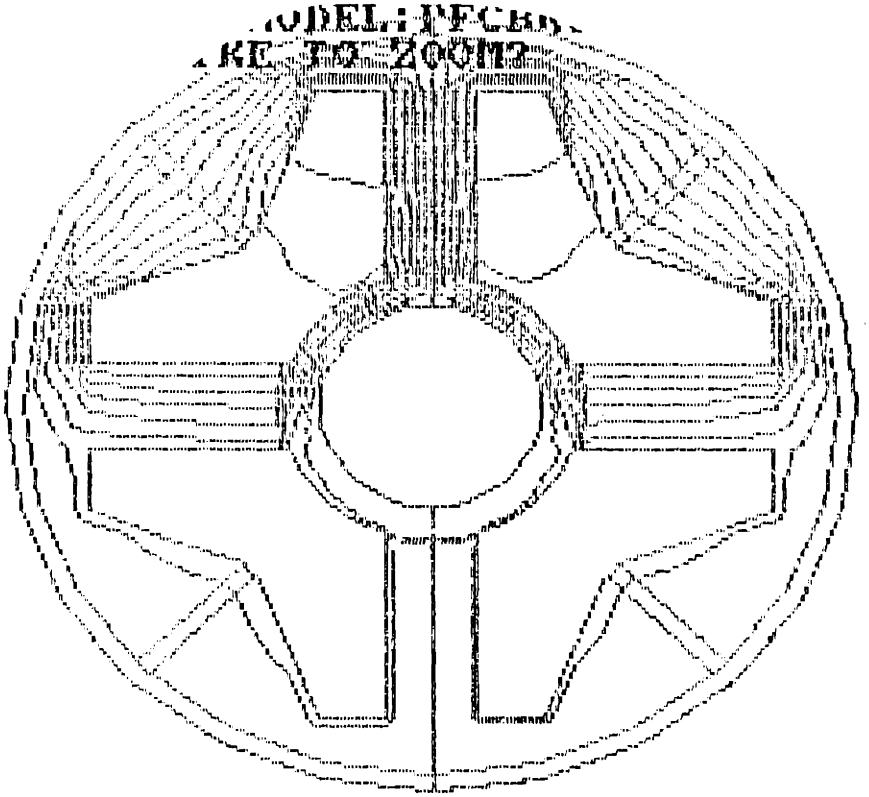

Figure 5.5 - Flux plot, One coil driven, no permanent magnets

Chapter 6: Circuit Analysis

This chapter contains the analysis developed in Chapter 2 applied to the specific Studor bearing tested. Equation 2.8 gives the relationship between gap flux density and net shaft force:

$$F = \frac{2 A \Delta B_c B_0}{\mu_0} \qquad (2.8)$$

To determine the force constant and negative spring constant of the bearing three things must be calculated. These are the initial operating flux density B_o, the function $\Delta B_c(I)$ (as a funciton of current), and the function $\Delta B_c(d)$ (as a function of displacement). This analysis will assume that the two ΔB_c functions are uncoupled, and that there is no leakage flux out of the magnetic circuits.

Looking at B_o first, it is determined by the intersection of the shearing line of the circuit and the demagnetizing curve of the magnets. The magnets in the bearing are made out of Samarium-Cobalt, a magnetically very hard rare earth material. They have a coercivity (H_c) of 716,000 A/m and a retentivity (B_r) of .965 tesla. According to Blah blah [8], Samarium-Cobalt is quite linear. Its demagentizing curve can be accurately modeled by a straight line between (0,-716,000) and (.965,0), which is given by:

$$B = 1.07 \mu_0 H + .965 \qquad (6.1)$$

where H is in A/m and B is in Tesla.

Now the shearing line must be calculated. From equation 2.5 the effective permeability can be calculated. Using the values (see appendix A for bearing dimensions) l_{air} = .003302 m, l_{iron} = .424 m, μ_{air} = 1, μ_{iron} = 4000, μ_e will be:

$$\mu_e = 125.57\ \mu_0$$

It will prove convenient to leave permeabilities in relative permeability form. Substituing l_m = .00635 m, l_T =.43434 m into eqation, 2.4 the relationship between B and H can be calculated (the shearing line slope).

$$\frac{B}{H} = -1.8632\ \mu_0 \qquad (6.2)$$

Combining 6.1 and 6.2, the initial flux can be determined.

$$B_0 = 0.628 \quad \text{Tesla}$$

This calculated initial flux density is slightly higher than the measured value of ≈.540 Tesla. This reflects one of two things. Either the leakage is significant, or the magnets were not fully saturated during their manufacture. Although the latter seems somewhat unlikely, some of the other data suggests this might be

the case (eg., finite element analysis). Samarium-Cobalt is an extremely hard material (magnetically), and it is not uncommon for them to be undersaturated.

With the inital flux density calculated, the next step is to attack the ΔB_c functions. By finding the dependence of ΔB_c on displacement, we can calculate the negative spring constant of the bearing. Although the magnet is quite linear, the relationship between the shearing line slope and dispalcement is not. It is most directly related to the effective permeability, μ_e, which is non-linear. By substituting l_{air} = .065" + g into equation 2.5, the following relationship between μ_e and gap size is obtained:

$$\mu_e = \frac{(0.065 + g + l_{iron})\,\mu_{air}\,\mu_{iron}}{(0.065 + g)\,\mu_{iron} + l_{iron}\,\mu_{air}} \qquad (6.3)$$

The derivative of μ_e with respect to gap is quite complicated. The easiest way to calculate $\Delta B_c(g)$ is to simply substitute a series of values around 0.065" (the initial gap length) into the equations and obtain the flux density for each one. Table 6.1 lists various gap sizes and their corresponding flux density.

Table 6.1: Gap flux desity for various gap sizes

Gap Length (in)	μ_e	B (T)	ΔB
0.080	113.08	0.6045	0.0234
0.075	116.89	0.6120	0.0159
0.070	121.10	0.6199	0.0080
0.065	125.57	0.6279	0.0
0.060	130.39	0.6361	0.0082
0.055	135.66	0.6446	0.0167
0.050	141.26	0.6532	0.0253

From this data we can deduce that B changes ≈0.0081 Tesla per .005" deviation from 0.065. Thus ΔB_c varies with gap size at a rate of roughly 1.62 Teslas per inch. By plugging this and the initial flux density of .628 T into equation 2.7 we obtain a negative spring constant 3,134 Newton's per inch, which equals 705 lbs/in. This value is lower than that found in testing by a factor of more than two. Since everything else points to values higher than the experimental, this suggests a flaw in this analysis.

This method assumed a constant circuit cross sectional area. The magnet, however, has an area of 5 square inches, while the gap has an area of 3 square inches. Since all of the flux lines from the magnet must go through the gap (assuming no leakage), the flux density in the gap will be 1.66 times greater in the gap than in the magnet. Multiplying the initial flux density by this factor gives a B_o of 1.05 Tesla, which more closely resembles the MAGGIE B_o for the same magnet parameters.

Finally, $\Delta B_c(I)$ must be calculated to get an analytical value for the force constant. Since gap flux is a linear function of current, this is much simpler than $\Delta B_c(g)$ and can be solved directly. Equation 2.3 states that:

$$B = \frac{N I}{A R} \qquad (2.3)$$

Differentiating this with respect to current gives:

$$\frac{d B}{d I} = \frac{N}{A R} \qquad (6.4)$$

which when combined with 2.3 gives:

$$\frac{d F}{d I} = K_f = \frac{2 B_0 N}{\mu_0 R} \qquad (6.5)$$

Using 0.540 T for Bo, 6.5 calculates a force constant of 0.293 N Newtons/Amp. (The experimental B_o is used since there is some ambiguity as to the theoretical value.) For the large windings this is 92.22 lbs/amp and 23.71 lbs/amp for the small windings. These values agree reasonably well with the experimental values.

To further check agreement between this analysis, MAGGIE, and the experiment, we can look at ΔB_c. Again using equation 2.3:

$$\Delta B_c = \frac{N I}{A R} = .2469\ I \qquad (6.6)$$

Thus, 1 amp of current will generate .2469 teslas of flux density. Maggie predicts the ΔB_c to be .251 teslas per amp, while experimentation predicts it to be between .24 and .27 teslas per amp. Thus both analysis methods and the experiments are close in aggreement, which points to magnet strength parameters as a large source of analysis errors.

The reluctance also can be used to calculate the inductance of the coils. Inductance is defined as the change in flux linkage per change in current. Flux linkage is proportional to the flux density, number of amp-turns, and the cross sectional area of the circuit. This reduces to equation 6.8:

$$L = \frac{N^2}{R} \qquad (6.7)$$

which shows that inductance is related only to the amp turns and the circuit reluctance. When the proper values are substituted into this equation, the calculated inductance for the 80% windings is 668 mH and 44 mH for the 20% windings. These match reasonably well with the experimental values.

Chapter 7: Conclusions and Recommendations

Looking at the data in light of the original objectives, many conclusions can be drawn. First is that the bearing is quite linear and non cross-coupled within the 0.003" range that it has been designed to operate in. The bearing showed only a few percent cross coupling at displacements of 0.020", indicating that it would also work well in a system with a much greater operating range, such as an actuated flexure system.

The coil inductances play a key role in determining the system bandwidth, however it is the system current driver that ultimately determines the frequency response. The dynamic performance can be improved with larger air gaps at the expense of force and negative spring constants. One way around this is through large permanent magnets, since they add working flux while increasing the effective air gap. The penalty for this solution is in weight and expense, as high energy product permanent magnets are neither light nor cheap.

Similarly it is the servo system that will determine the suspension's maximum capacity and/or stiffness. The servo perfomace can be enhanced by designing the bearing for maximum force and negative spring constants, thus lessening power supply needed for a given capacity.

The two axis testing was good conceptually, however it suffered in practice from lack of test apparatus stiffness. In future

testing it is recommended that the rig be designed to be as stiff as possible, preferably with two single axis load cells as opposed to a single multi-axis cell. A heavy shaft mount is essential. Unfortunately the using a jig borer makes this difficult to achieve. A two axis slide similar to the single axis apparatus would work far better.

Dynamic testing should be done in the form of frequency response methods. The transfer function analyzer provided a 'cleaner' curve than the white noise and spectrum analyzer combination. Reactance methods are satisfactory as a rough cut, but should be done only within the device's operating bandwidth.

The analysis also showed some encouraging results. The gap flux density changes from the electromagnets matched well between the experiment and both analysis types. Since the magnet parameters were never measured, the validity of the absolute constant analysis cannot be ascertained. Since the electromagnet data seems to match so well, the permanent magnet parameters come under suspicion. These parameters must be measured before bearing assembly. Despite this problem, MAGGIE seems to be an invaluable tool in magnetic analysis, and circuit analysis provides a good rough cut for doing preliminary design.

References

1. Hamilton, Brian J., "Magnetic Suspension: The Next Generation in Precision Pointing".
2. Meeks, C.R., ,Hughes Aircraft Company,1986.
3. Geary, P.J., Magnetic and Electric Suspensions, British Scientific Instrument Research Association, 1964.
4. Backers, F.T., "A Magnetic Journal Bearing", Phillips Technical Review, Apr. 5, 1961.
5. Studer, Phillip A., and Wilson, Meredith, "Linear Magnetic Bearings", paper #V-4 at the 5th International Workshop on Rare-Earth Cobalt Magnets and Their Applications, Roanoke, VA, June, 1981.
6. "Prototype Flight Cooler and Component Demonstration, Quaterly Program Review", Hughes Aircraft Co., Sept. 10, 1986.
7. Kraus, John D., Electromagnetics, McGraw-Hill, 1984.
8. Heck, Carl, Magnetic Materials and Their Applications, Butterworth and Company, 1974.

Appendix A: Dimensions of PFC demo bearing

The following drawings are reductions of the production drawings for the bearing tested in this thesis. Although it not the complete set, all the critical dimensions for analysis can be found on these drawings.

REV	DESCRIPTION OF CHANGE	DRAWN	APP'D	DATE	DCN NO
B	DCN 86-857				
C	DCN 86-899				AC-562
A	DIM				

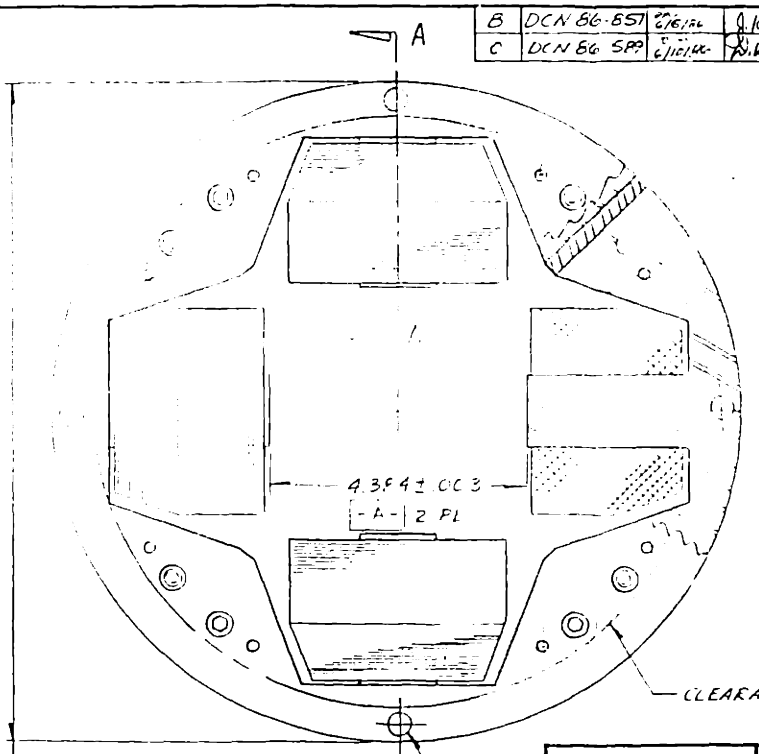

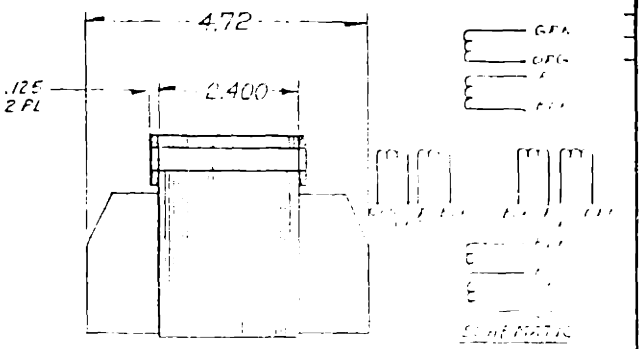

SECTION A-A

OPERATING RANGE DATA	COIL A	COIL B	
LEAD COLORS	WHITE-RED	ORANGE-BLACK	
PEAK FORCE (F_P)	20	80	LBS
FORCE CONST (K_F)	10	40	LBS/AMP
BACK EMF CONST (K_E)	13.6	54	VOLTS/FT/SEC
MOTOR CONST (K_M)	20.4	21.1	LBS/√WATTS
RESISTANCE (R) @ 25°C	.93	3.6	OHMS

ϕ 11.000 $^{+.000}_{-.002}$ MTG HOLE
ϕ.3750 $^{+.0005}_{-.0000}$ THRU
4 EQ SP ON ϕ10.375 ± .002 EC

⊚	ϕ.002	A

⌖	ϕ.014	A

NOTES: (UNLESS OTHERWISE SPECIFIED)

DIMENSIONS SHOWN ARE AFTER PLATING
TOLERANCE UNLESS OTHERWISE SPECIFIED
LINEAR .XXX = ± .005 .X = ± .010
.X = ± .030 ANGULAR = ± 0°30'
SURFACE ROUGHNESS
FINISH ALL SURFACES NOT OTHERWISE SPECIFIED
REMOVE ALL BURRS
BREAK ALL SHARP EDGES

MATERIAL	PLATING	HEAT TREAT	DWG SIZE
			B

CODE IDENT. NO	SCALE	
55789	N/A	5/6/86

1 INCH = 25.4 MM

DIM'S SHOWN IN INCHES

TITLE: MAGNETIC BEARING

KIMCO DIVISION
SAN MARCOS, CA 92069

MB105-47-001

REV	DESCRIPTION OF CHANGE	DRAWN	APP'D	DATE	DCN NO
A	2 COILS, DIM'S, DATA	[illegible]	[illegible]	5/21/86	86-570

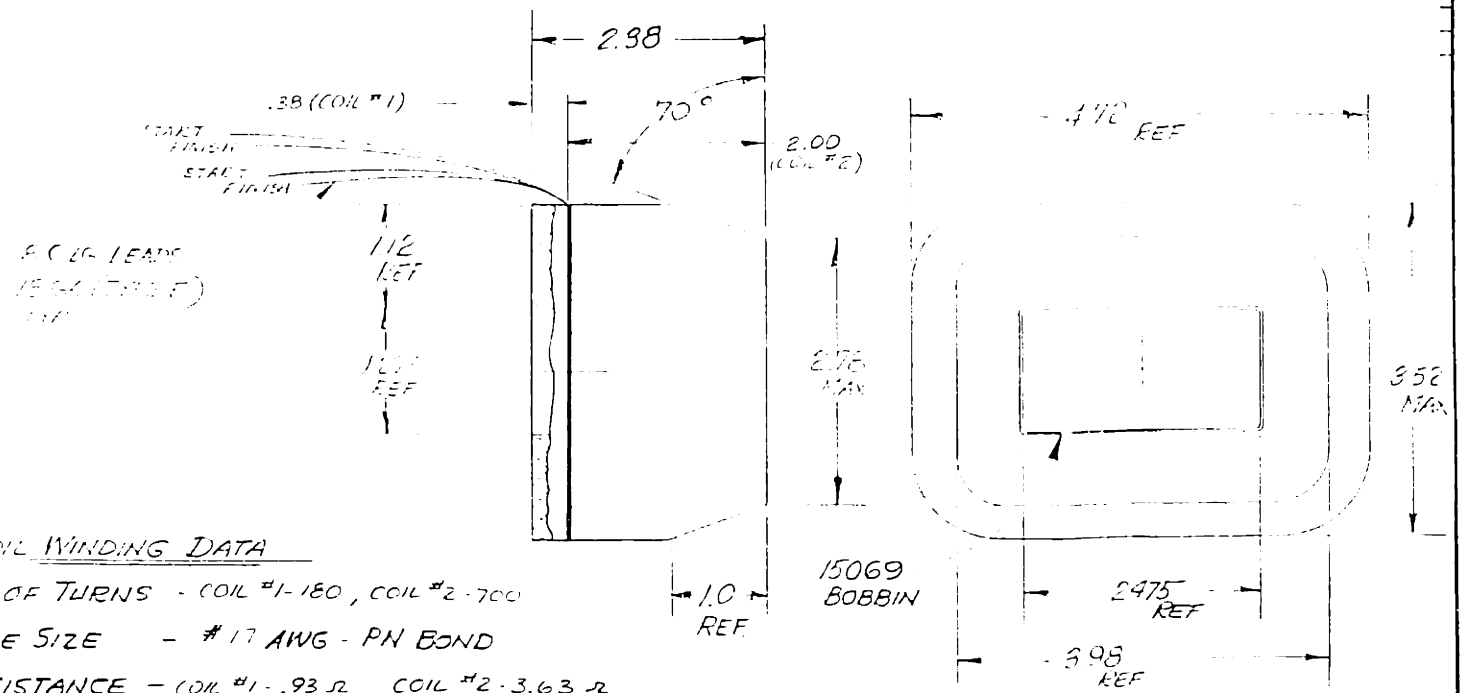

COIL WINDING DATA

NO. OF TURNS - COIL #1 - 180, COIL #2 - 700

WIRE SIZE - #17 AWG - PN BOND

RESISTANCE - COIL #1 - .93 Ω, COIL #2 - 3.63 Ω

NOTES: (UNLESS OTHERWISE SPECIFIED)

DIMENSIONS SHOWN ARE AFTER PLATING

TOLERANCES UNLESS OTHERWISE SPECIFIED

SURFACE ROUGHNESS FINISH ALL SURFACES NOT OTHERWISE SPECIFIED

REMOVE ALL BURRS

BREAK ALL SHARP EDGES

MATERIAL	PLATING	HEAT TREAT	DWG SIZE
			B

CODE IDENT NO.	SCALE	DRAWN	APP'D
55789	1:1	[illegible] 5/6/86	

1 INCH = 25.4 MM

DIM'S SHOWN IN INCHES

TITLE: COIL ASS'Y

KIMCO DIVISION
SAN MARCOS, CA 92069

15070

REV.	DESCRIPTION OF CHANGE	DRAWN	APP'D	DATE	DCN NO

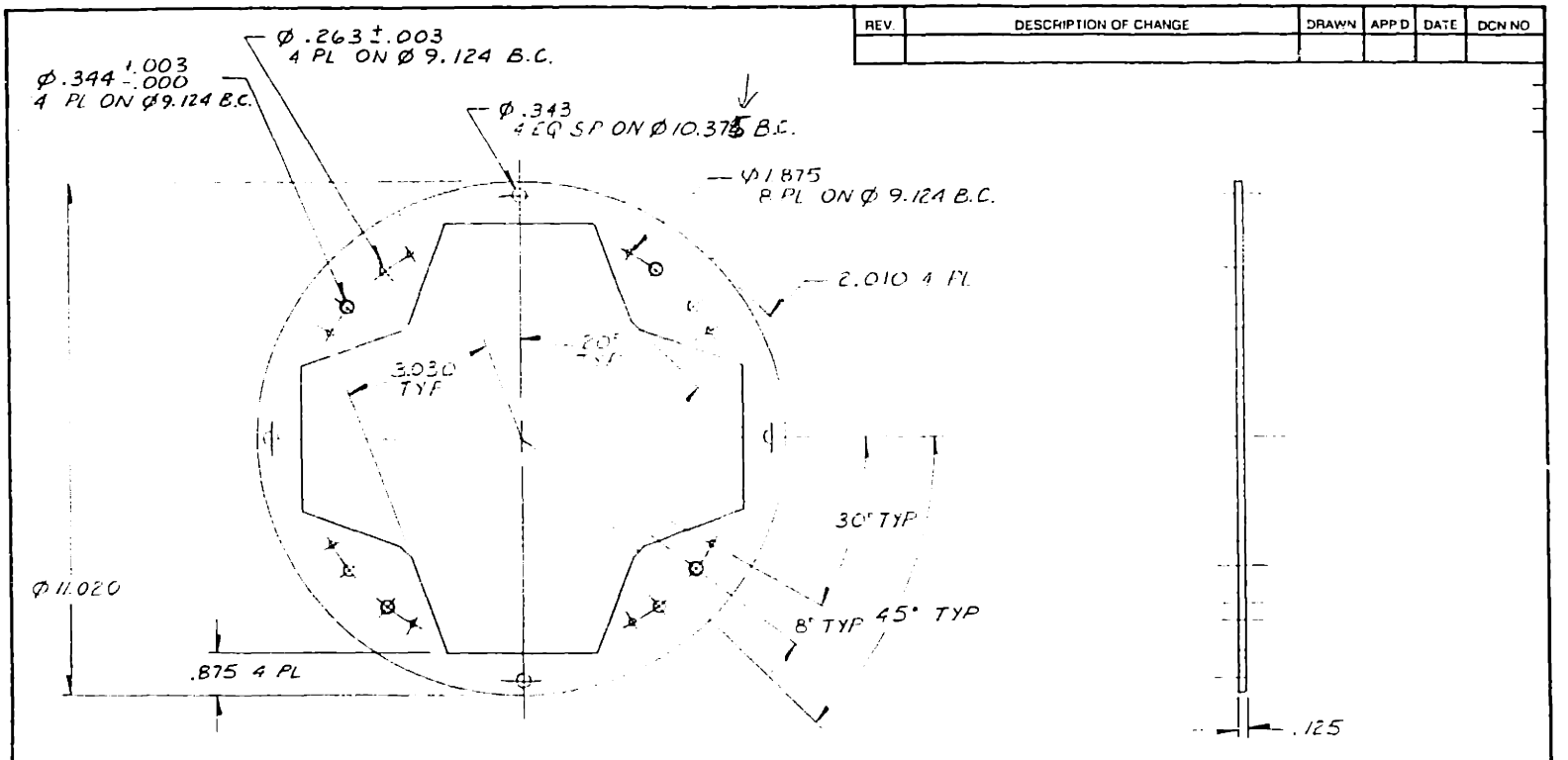

NOTES: (UNLESS OTHERWISE SPECIFIED)

DIMENSIONS SHOWN ARE AFTER PLATING
TOLERANCES UNLESS OTHERWISE SPECIFIED
LINEAR .XX = ±.01 .XXX = ±.005
X = ±.030 ANGULAR = ±1°
SURFACE ROUGHNESS
FINISH ALL SURFACES NOT OTHERWISE SPECIFIED:
REMOVE ALL BURRS
BREAK ALL SHARP EDGES

MATERIAL 303 S.S.	PLATING		HEAT TREAT	DWG SIZE B
CODE IDENT NO 55789	SCALE 1/2	DRAWN J. Gonzalez 4/28/92		
1 INCH = 25.4 MM		APP'D J.K. 5/6		
DIM'S SHOWN IN INCHES	TITLE END PLATE			

BE KIMCO DIVISION SAN MARCOS CA 92069

09057

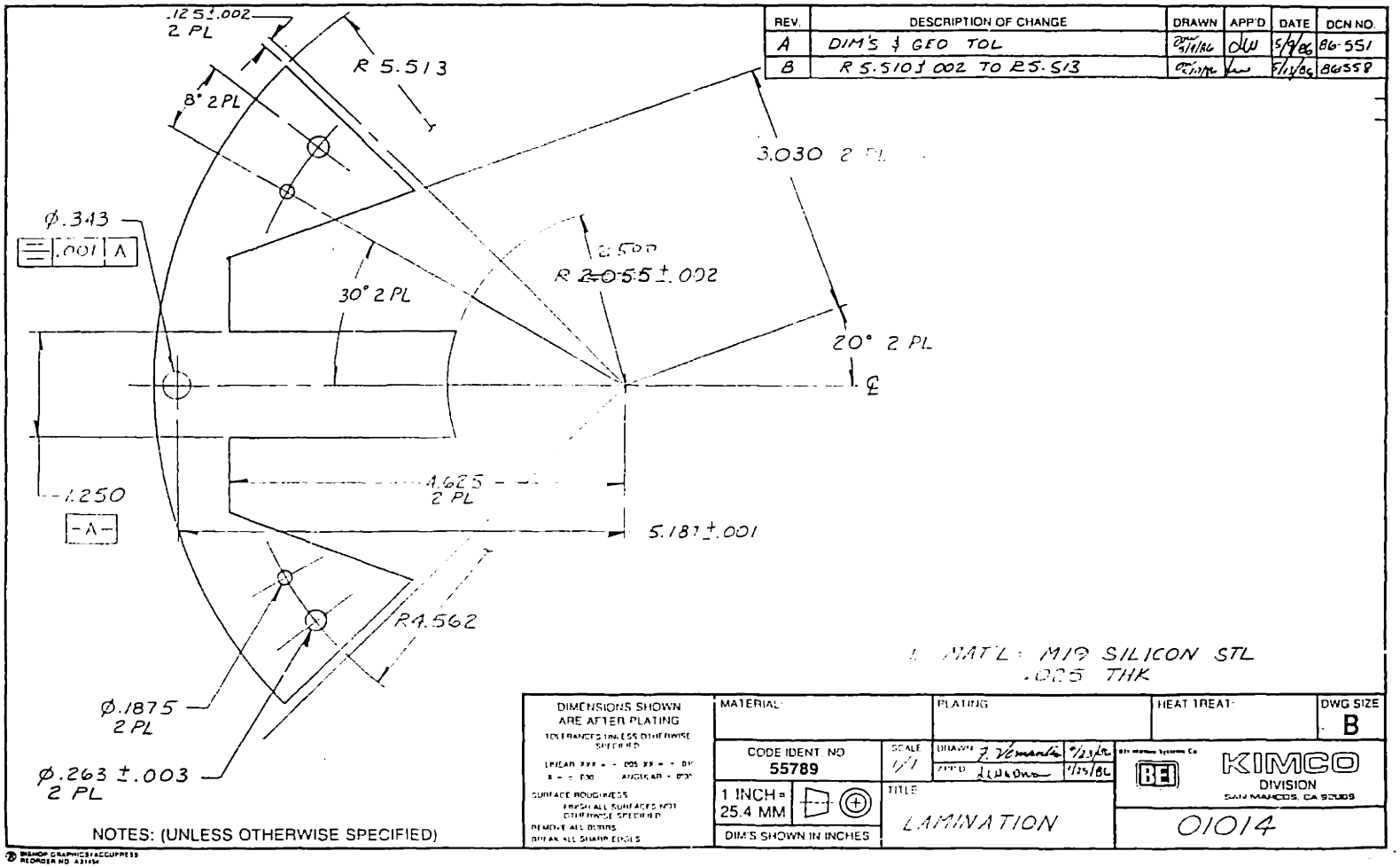

REV.	DESCRIPTION OF CHANGE	DRAWN	APP'D	DATE	DCN NO.
A	DIM'S & GEO TOL	4/11/86	DW	5/9/86	86-551
B	R 5.510 ± .002 TO R 5.513	[illegible]	[illegible]	5/14/86	86-558

NOTES: (UNLESS OTHERWISE SPECIFIED)

1. MAT'L: M19 SILICON STL
.005 THK

DIMENSIONS SHOWN ARE AFTER PLATING

TOLERANCES UNLESS OTHERWISE SPECIFIED

LINEAR .XX = ± .005 .XX = ± .01
X = ± .030 ANGULAR = ± 1°

SURFACE ROUGHNESS
FINISH ALL SURFACES NOT OTHERWISE SPECIFIED

REMOVE ALL BURRS
BREAK ALL SHARP EDGES

MATERIAL	PLATING	HEAT TREAT	DWG SIZE
			B

CODE IDENT. NO. 55789	SCALE 1/1	DRAWN J. Hernandez 4/23/86	KIMCO DIVISION SAN MARCOS, CA 92069
1 INCH = 25.4 MM		APP'D [illegible] 4/25/86	
DIM'S SHOWN IN INCHES	TITLE LAMINATION		01014

BISHOP GRAPHICS/ACCUPRESS REORDER NO. A3164

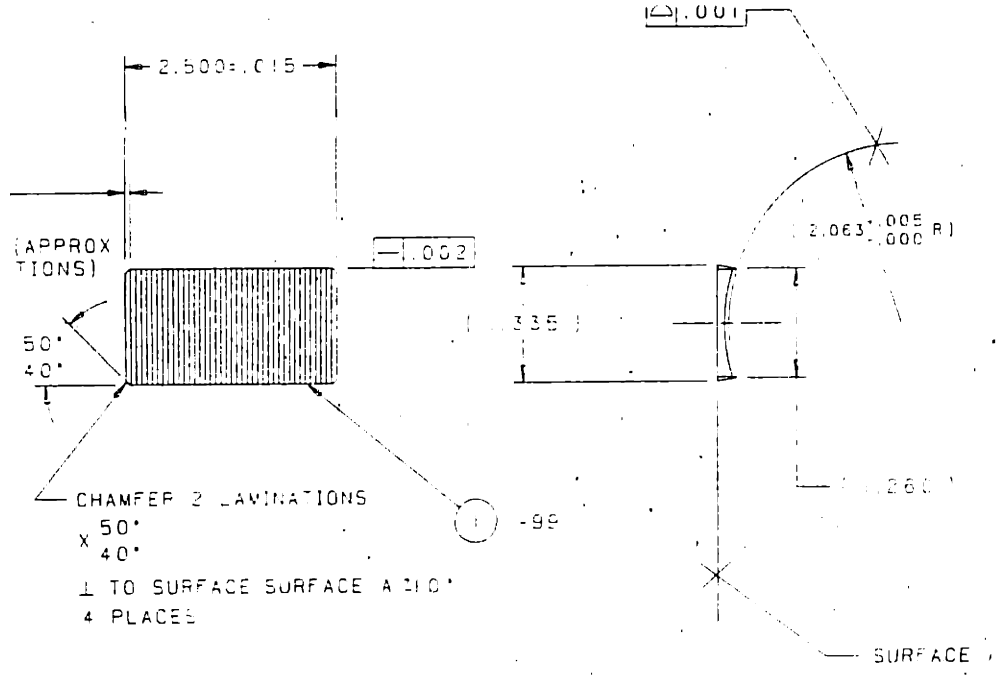

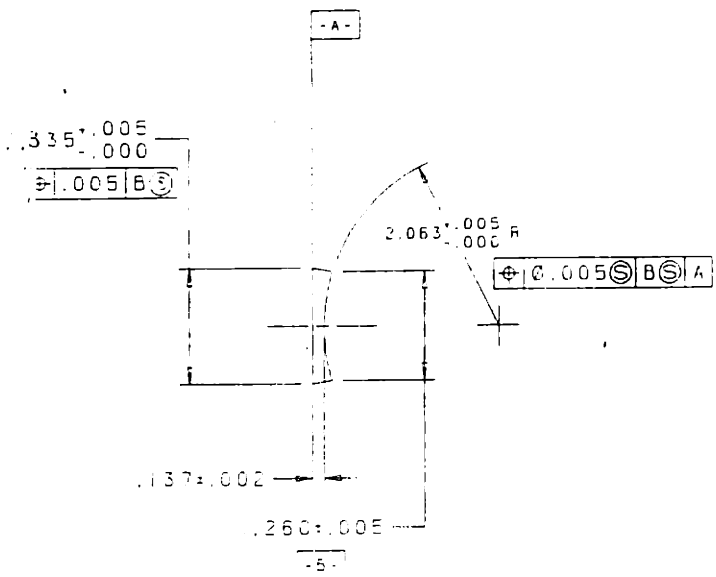

-99

(SINGLE LAMINATION)

A/R	
QTY REQD	FSC

UNLESS OTHE
DIMENSIONS
AND PER
.XXX
±.010

MATERIAL

AISI
SILIC

6252905	
NEXT ASSY	USED ON

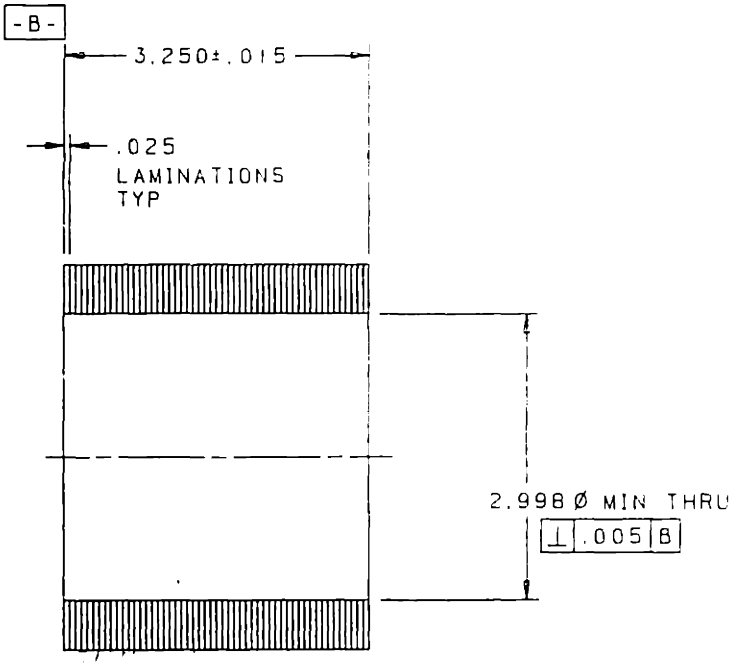
-B-
3.250±.015
.025
LAMINATIONS
TYP
2.998 Ø MIN THRU
⊥ .005 B

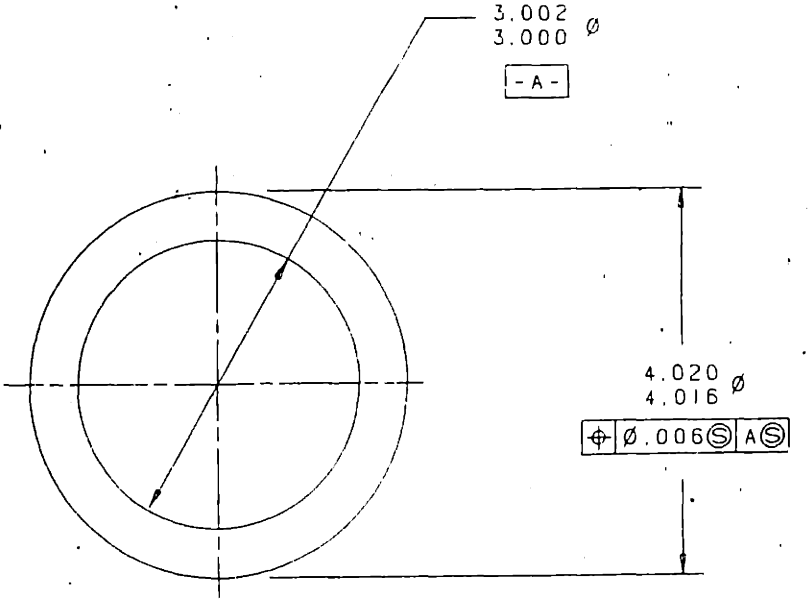
3.002
3.000 Ø
-A-
4.020
4.016 Ø
⌖ Ø.006Ⓢ AⓈ

DETAIL -99